INTERSYMBOL INTERFERENCE (ISI) MITIGATION SCHEMES IN IR-UWB SYSTEMS EMPLOYING ENERGY DETECTION RECEIVER

by

Atheindhar Viswanathan Rajendran

Submitted
in partial fulfilment of the requirements
for the degree of Master Of Applied Science

at

Dalhousie University
Halifax, Nova Scotia
April 2013

DALHOUSIE UNIVERSITY

DEPARTMENT OF ELECTRICAL AND COMPUTER ENGINEERING

The undersigned hereby certify that they have read and recommend to the Faculty of Graduate Studies for acceptance a thesis entitled "INTERSYMBOL INTERFERENCE (ISI) MITIGATION SCHEMES IN IR-UWB SYSTEMS EMPLOYING ENERGY DETECTION RECEIVER" by Atheindhar Viswanathan Rajendran in partial fulfilment of the requirements for the degree of Master of Applied Science.

Dated: April 17, 2013

Co-Supervisors: _____
Dr. Zhizhang (David) Chen

_____
Dr. Hong (Jeffrey) Nie

Readers: _____
Dr. Jose Gonzalez-Cueto

_____
Dr. William Phillips

DALHOUSIE UNIVERSITY

DATE: April 17, 2013

AUTHOR: Atheindhar Viswanathan Rajendran

TITLE: INTERSYMBOL INTERFERENCE (ISI) MITIGATION SCHEMES IN IR-UWB SYSTEMS EMPLOYING ENERGY DETECTION RECEIVER

DEPARTMENT: Department of Electrical and Computer Engineering

DEGREE: M.A.Sc CONVOCATION: October YEAR: 2013

_____

Signature of Author

TABLE OF CONTENTS

LIST OF TABLES

LIST OF FIGURES

ABSTRACT

Ultra-Wideband (UWB) is an emerging wireless technology that has attracted many applications in modern day communications. Its ability to provide high data rates at very low complexity makes the system attractive for many indoor high-speed wireless communications. UWB signal can be transmitted by either impulse radio (IR) or multicarrier techniques. Impulse radio technique in particular, is a carrier less technology using pulses in the range of nanoseconds or less providing a low complexity, low power and low interference susceptible wireless system. These features motivate the usage of energy detection based receiver structures that operates at very low power.

With the recent developments in UWB technology, a promising feature of this system is to provide high data rate with transceivers operating at very low power. High data rate on the other hand can be achieved only by using a complex modulation schemes that requires more transmitted power. As a limitation in the spectral emission associated with UWB, only low-level modulation technology can be used in UWB systems. Hence, in order to achieve high data rates using low-level modulation schemes, the Inter-symbol interference (ISI) becomes unavoidable.

Decision feedback equalization (DFE) is one of the signal process techniques that can be used to mitigate the effects of ISI. This thesis proposes an energy subtraction algorithm combining with the principles of DFE to mitigate the effects of ISI in an impulse radio UWB system employing energy detection receiver. Computer simulations have been performed to verify the operation of the new proposed algorithm under UWB channel characteristics and relevant comparisons have been made with the basic energy detection receiver. Simulation results show that the ISI can be effectively mitigated with low system complexity.

LIST OF ABBREVIATIONS USED

2PPM	Binary Pulse Position Modulation
A-RAKE	All Rake
AWGN	Additive White Gaussian Noise
BER	Bit Error Rate
BPF	Band Pass Filter
CIR	Channel Impulse Response
CSR	Code Shifted Reference
DCSR	Differential Code Shifted Reference
DFE	Decision Feedback Equalization
EDR	Energy Detection Receiver
EIRP	Effective Isotropic Radiated Power
FCC	Federal Communication Commission
FM	Frequency Modulation
FSR	Frequency Shifted Reference
IR	Impulse Radio
ISI	Intersymbol Interference
LOS	Line-Of-Sight
LTI	Linear Time Invariant
MB	Multiband
MC	Multi Carrier
MIR	Micro Power Impulse Radar
MLSE	Maximum Likelihood Sequence Estimation
MPC	Multipath Component
MSE	Mean Square Equalizer
NLOS	Non Line-Of-Sight
OFDM	Orthogonal Frequency Division Multiplexing
PPM	Pulse Position Modulation
PSD	Power Spectral Density
RF	Radio Frequency

RMS	Root Mean Square
S-RAKE	Selective Rake
SBS	Symbol-By-Symbol
SE	Sequence Estimation
SNR	Signal To Noise Ratio
TR	Transmitted Reference
UWB	Ultra-Wideband
WPAN	Wireless Personal Area Network

ACKNOWLEDGEMENTS

First and foremost, I would like to express my deepest sense of gratitude to my Guru and Supervisor, Dr. Zhizhang (David) Chen for his patient guidance, valuable advice and for providing me with tremendous technical and moral support. His words of wisdom have been a true motivating factor for the completion of this thesis. I feel so proud to have worked with him for giving me a memorable experience at the RF/Microwave Research Laboratory. I would like to extend my gratitude to my second Guru, Co-Supervisor, Dr. Hong Nie from University of Northern Iowa, for his valuable advice and suggestions. I really appreciate for the countless times that he spent on providing feedback on my work.

I would like to thank my friends and colleagues from the RF/Microwave Research Laboratory for supporting this research work. I must also thank my committee members, Dr. Jose Gonzalez Cueto and Dr. William Phillips for their interest in this research work and providing me with invaluable support to carry out my work. Specially, I would like to thank Dr. Jose Gonzalez Cueto for providing me teaching assistantships during my degree and helped me gain immense experience with his laboratory classes.

Nothing would have happened without my parents support. They have been my heart and soul throughout the journey of this research work. I would like to specially thank my father who inspired me to be a successful person in life and for providing me an opportunity to pursue my degree in Canada. Above all, it was with the help of Almighty, Lord Krishna who blessed me with courage and infinite energy to surpass every hurdle in my life and helped me realize my goals during the course of this research.

ALL IS WELL

CHAPTER 1: INTRODUCTION

This Chapter gives a brief introduction of the history of Ultra-Wideband (UWB) communication, and then introduces the thesis by providing the research motivations and thesis outline.

1.1 Historical Background

With the development of Linear Time Invariant (LTI) systems, the UWB is generally perceived to have started after the year 1960. But the history of UWB can be traced back to the year 1886, when Hertz tried to solve Maxwell's equations and realized two spark generators. Hertz, as a physicist, was only interested in solving Maxwell's equations, but he did not realize the potential of spark gap transmissions at that time [1]. It was his ideas that inspired Marconi to invent a wireless radio transmission system with Hertzian waves. In the year 1895, Marconi, the first wireless transmission engineer in history, set up the first experimental apparatus for the first wireless transmission.

The usage of wireless apparatus became so common until the beginning of the 20^{th} century where the first problem arose. It was then found that these spark gap transmissions occupied a large part of the radio spectrum, and also they were so heavy to carry and consumed a lot of power.

In the late 1960's, contributions made by Henning F. Harmuth at the Catholic University of America, Paul van Etten at the Air Development Center in Rome, and Ross and Robbins at the Sperry Rand Corporation, renewed interests in UWB technology. However, it became difficult for the impulsive techniques associated with LTI systems, in which the impulsive units became difficult to realize with quick time measurement constraints. Later, in the year 1962, with the advent of the sampling oscilloscope and

development of sub-nanosecond technology, the impulse response was measured and observed with sufficient accuracy.

Several researches were carried since then, but still UWB communication systems were lacking sensible receivers until 1972, when the invention of the short pulse receiver (Robbins 1972) replaced the bulky time domain oscilloscopes. On 17th April 1973, the new modern UWB system was born when Ross filed an US Patent, "Transmission and reception system for generating and receiving base-band pulse duration pulse signals without distortion for short base-band communication system'' [1].

Later in the 20th century, during 1980's, researches started naming UWB technology with alternative names such as impulse, carrier free or baseband systems. It was then in the year 1989, the U.S Department of Defense coined the term " Ultra-Wideband", and by then Sperry had filed almost 50 patents in the field of UWB covering various transmitters, receivers and pulse generation systems [1]. All these patents covered extensive applications starting from radars to communication and positioning systems. Some patents also included applications related to liquid level sensing, altimetry and other vehicle collision avoidance systems. Inspired from the works of Ross, in the year 1994, McEwan built the "Micro power Impulse Radar" (MIR), operating at a very low voltage: in fact, it used a 9V battery. This MIR used sophisticated signal processing techniques and receiving methods that made it extremely compact and inexpensive.

Apart from the original time domain Impulse Radio Ultra-Wideband (IR-UWB), several other alternative schemes emerged like the Multi Carrier (MC-UWB), Orthogonal Frequency Division Multiplexing (OFDM-UWB) and Frequency Modulation (FM-UWB). After attaining great developments in the sub-nanosecond technology starting from 1960 until the end of the century, there came the urgency for worldwide activities to end up with an UWB standardization process. A significant milestone happened in the year 2006 when there were different UWB physical layers in consideration to be formed

as the basis of the IEEE 802.15.3a standard. After several years of wrangling from different parties, all the groups had given up on this standardization. The IEEE 802.15.3a working committee then decided to disband the group on January 19, 2006 at a meeting in Hawaii [1].

1.2 Motivation

Conventional narrowband techniques were completely dominating the wireless transmission systems in the past. Though these narrowband wireless systems found themselves applicable in a broad range of applications, they failed to meet the demand of high data delivery to the end user. A characteristic of narrowband transmission was the limitation in bandwidth that in turn capped the limit on transmission capacity. The wireless market started growing exponentially, causing high demands in accommodating more users and in achieving high data rates.

Overcoming the bandwidth limitations, UWB technology started gaining significant importance in the wireless industry. UWB communication is based on transmission of a short pulse with very low energy and very high bandwidth, making it a strong candidate in areas of wireless industry requiring accommodation of more users. It also helps in achieving very high data rates. Due to the characteristic of having very high bandwidth, UWB waves have good material penetration capability and also the UWB technique has fine time resolution, finding its application in positioning and ranging. These powerful applications of UWB were used for military purposes for several years until the Federal Communications Commission (FCC) approved the usage of an unlicensed UWB spectrum for wireless communications, and this opened the door for new potentials. Since then, UWB technology has witnessed a tremendous increase in research from both academic and industrial organizations.

The distinct feature of having an ultra-wide bandwidth makes it advantageous over the conventional narrowband systems, providing very high data rates and accommodating more users. Furthermore, IR-UWB is a carrier-less technology implying that a mixer is not required. This omission of a mixer makes the construction of a UWB transmitter/receiver so simple, and hence the cost is brought down as compared to that of the conventional Radio Frequency (RF) carrier systems.

High data rates and low transmission power are the two promising features of impulse radio UWB. This technology can be implemented either by using coherent or non-coherent receivers, where the latter is said to be powerful in developing low complex receiver designs. To distinguish briefly between the two designs: a coherent receiver is required if using a system with a very high data rate and good Bit Error Rate (BER) levels. On the other hand, simpler architectures and low power are the two main characteristics of the non-coherent receiver designs [2][3]. Due to the simplicity in design, the non-coherent receivers are more suitable for impulse radio UWB as they offer low cost, low complexity, and also find themselves in a variety of applications where low power is much needed [4][5].

Energy detectors were then used to implement the non-coherent receiver designs [6]. More details on energy detectors are discussed in Chapter 3, where different receiver structures using different modulation schemes use the concept of energy detection. In literature there are a number of solutions proposed to implement IR-UWB, like the Transmitted Reference (TR), Frequency Shifted Reference (FSR), Code Shifted Reference (CSR), Differential Code Shifted Reference (DCSR) and the Pulse Position Modulation (PPM) based on energy detection principles. They will be described in more detail in Chapter 3. The concept of an energy detection-based PPM impulse radio UWB receiver forms the basis of this thesis.

Even though energy detectors are best suitable for low complex and low power designs, they are often more susceptible to Intersymbol Interference (ISI). This is a problem when a pulse does not die out completely before the detection of the next incoming pulse, thereby causing unnecessary overlapping of pulses leading to errors. Several research works have been carried out in the past to mitigate the effects of ISI in a PPM based energy detector [7] where complex back end signal processing algorithms were adopted, raising the system complexity. Therefore, this thesis proposes a couple of simple efficient algorithms to cancel the effects of ISI and also maintain low system complexity.

1.3 Thesis Outline

This thesis is organized as follows:

Chapter 2: UWB Radio Technology: A general overview of UWB Technology, its definition, applications, and types of UWB systems are dealt in this chapter. General characteristics of the channel model considered in this thesis are also presented at the end of this chapter.

Chapter 3: Implementation Schemes for IR-UWB: The receiver designs for IR-UWB and their working philosophies including Rake Receiver, Transmitted Reference (TR), and Frequency Shifted Reference (FSR) are explained. This chapter also introduces the working concept of energy detection and the receiver structure based on Pulse Position Modulation employing energy detection (ED-PPM).

Chapter 4: Intersymbol Interference (ISI) and Traditional Signal Processing: This chapter introduces the problem of ISI in general. Some traditional methods of ISI mitigation schemes are also discussed.

Chapter 5: Signal Processing in ED-PPM: Proposed schemes and Comparisons: An in-depth study of the performance metrics (BER) in a PPM-ED under different ISI conditions is explained. Two simple ISI mitigation algorithms are proposed and their BER performances are compared with the traditional PPM-ED system. A detailed

comparison table is then provided at the end of the chapter covering all points from system performance to complexity for all the new and old schemes with the inclusion of an alternate design to ED-PPM.

Chapter 6: Conclusions and Future Work: This chapter gives an overall summary of the thesis as well as the future work recommended and discussed.

Appendix contains the MATLAB code used for the ED-PPM based on energy subtraction algorithms, and References are listed at the end of the thesis.

CHAPTER 2: UWB RADIO TECHNOLOGY

2.1 Overview

The history of UWB technology dates back to nearly one hundred years ago, when Marconi first initiated wireless transmission using spark gap transmitters from the Isle of Wright to Cornwall on the British mainland. Deployment of UWB technology was widely practiced during the period of 1960 to 1990. The first use of UWB technology was ground penetrating radar developed by the United States Military. Since then, the FCC realized the importance of UWB technology, and in the year 1998 they initiated a regulatory review process of this technology. It was then in the year 2002, on February 14, the FCC authorized UWB technology for commercial uses covering a variety of applications, and provided detailed information on the unlicensed operating frequency bands as well as the transmitted power spectral densities [8].

UWB signals can be classified into two main categories: IR-UWB, also called the single band technology which resembles earlier spark gap transmissions, and Multi-Band Orthogonal Frequency Division Multiplexing (MB-OFDM), which uses multiple frequency bands for UWB signaling.

UWB has a very wide bandwidth of more than 7GHz and uses frequencies from 3.1GHz to 10.6GHz, where each radio channel can have a minimum bandwidth of 500MHz or more. The FCC then put power restrictions into place in order to handle this very large bandwidth without affecting or interfering with the other existing narrowband techniques. Since the FCC had implemented these power restrictions, UWB radios had to be designed to operate at very low power and hence UWB devices were designed for very low power transmissions. It became effective to produce these low power devices using cost effective CMOS implementations. All of these UWB characteristics of having low operating power, low cost and low complexity found, were then used in various applications, especially in Wireless Personal Area Networks (WPAN's).

2.2 UWB Definition & FCC Regulations

According to the FCC, UWB transmission is defined as any radio signal that has a fractional bandwidth (B_f) larger than 20%, or which occupies a bandwidth of 500MHz or more, i.e.,

$$BW = (f_H - f_L) \geq 500 MHz \tag{2.1}$$

or,

$$B_f = \frac{BW}{f_c} = \frac{(f_H - f_L)}{(f_H + f_L)/2} \geq 20\% \tag{2.2}$$

where B_f is the fractional bandwidth, defined as the ratio of signal bandwidth to the center frequency, f_H and f_H are the upper and lower transmitted frequencies at the -10dB emission point, and f_c is the center frequency defined as,

$$f_c = \frac{(f_H - f_L)}{2}$$

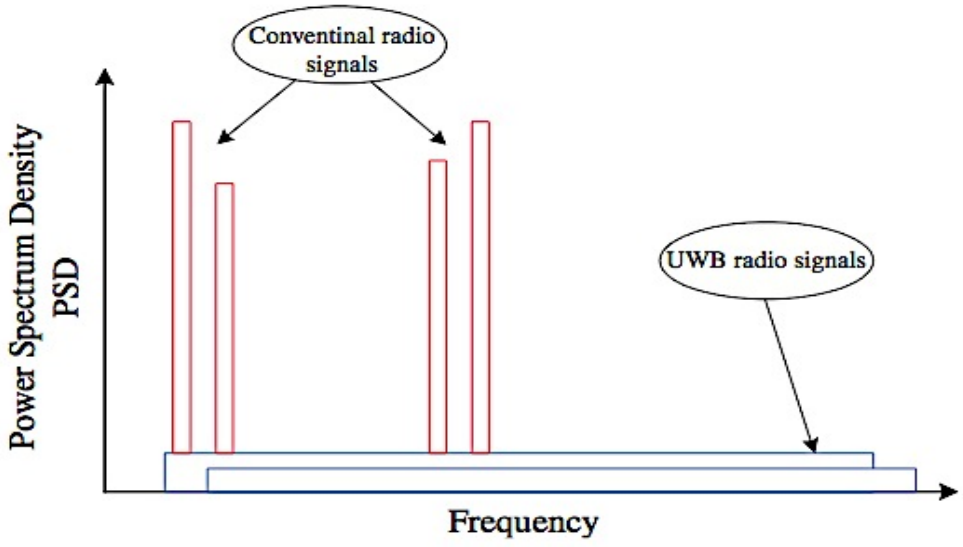

Figure 2-1 : Conventional radio signal versus UWB signal [1]

As shown in Figure 2-1, the conventional radio signals have fractional bandwidths of less than 5%.

In order to avoid interference with existing wireless communication systems, various regions of the UWB spectrum should have different power spectral densities. Hence, in the year 2002, the FCC defined a set of rules and recommendations for UWB devices to work in a specific power spectral density (PSD) mask. This PSD level is set to -41.3 dBm for the frequency range of 3.1GHz to 10.6GHz so as to limit the interference with the existing wireless communication systems, and also to protect existing radio services. Additionally, the FCC proposed two masks, one for indoor UWB devices and the other for outdoor UWB devices where the radiation limits are similar to each other.

The indoor FCC spectral mask is shown in Figure 2-2; while for the 1.6GHz to 3.1GHz frequency range, the outdoor mask is 10dB lower than the indoor mask and is shown in Figure 2-3.

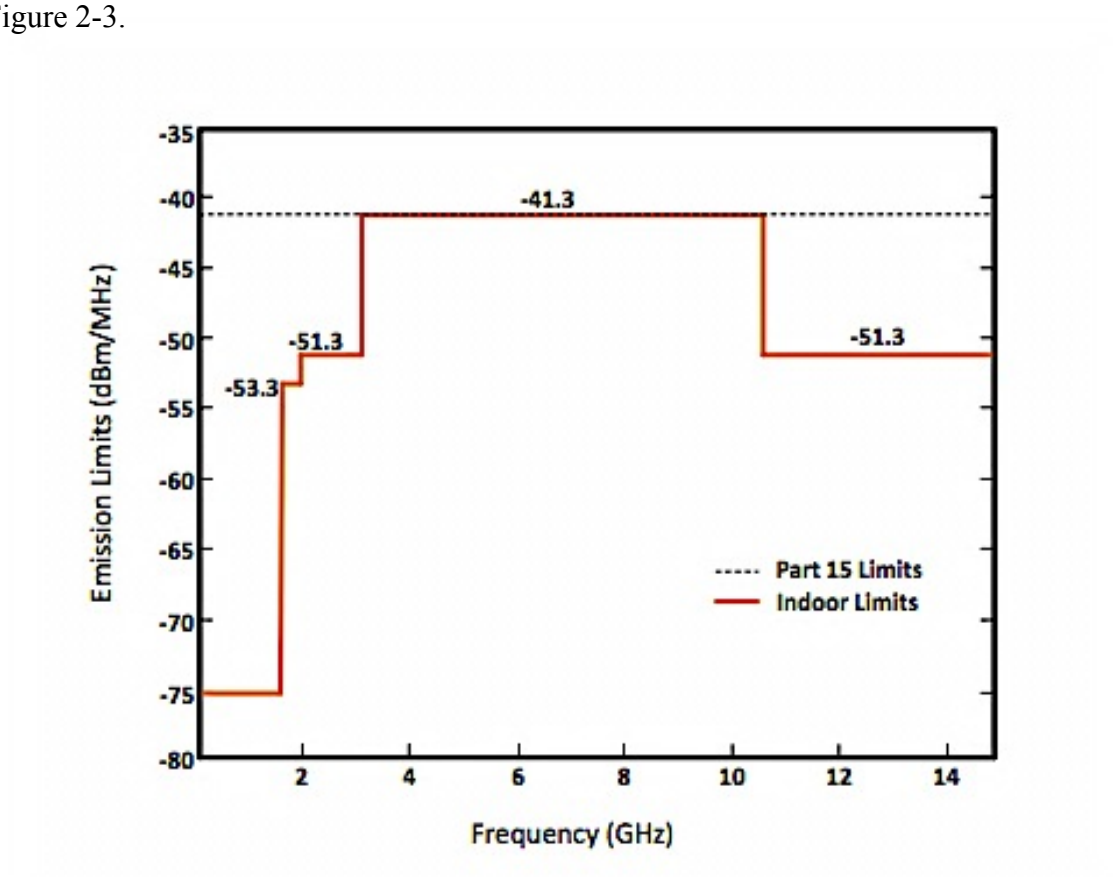

Figure 2-2 : FCC Emission Limits for Indoor UWB Communications

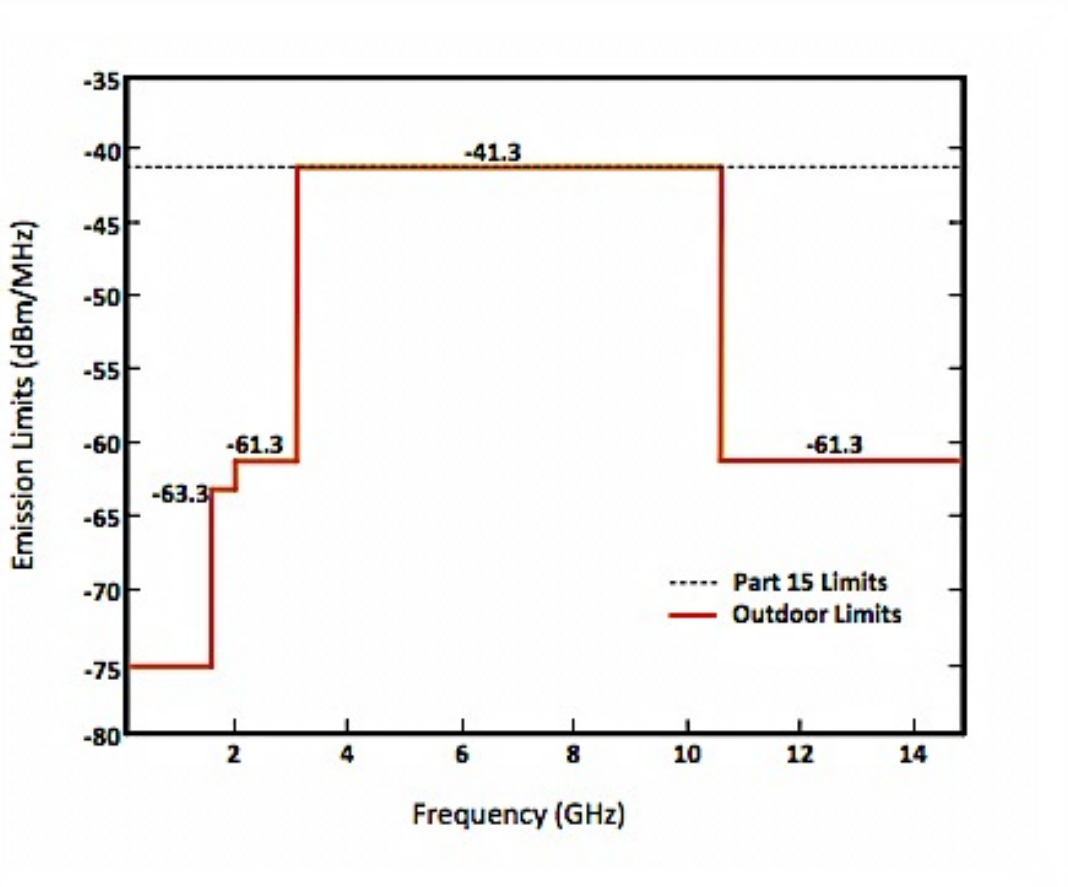

Figure 2-3: FCC Emission Limits for outdoor UWB Communications

The table below summarizes FCC Spectral Emission masks for both indoor and outdoor UWB communications.

Table 2-1: FCC Emission Limits for Indoor and Outdoor UWB [1]

Frequency Ranges	Indoor EIRP (dBm/MHz)	Outdoor EIRP (dBm/MHz)
960 MHz – 1.1 GHz	-75.3	-75.3
1.61 GHz – 1.99 GHz	-53.3	-63.3
1.99 GHz – 3.1 GHz	-51.3	-61.3
3.1 GHz – 10.6 GHz	-41.3	-41.3
Above 10.6 GHz	-51.3	-51.3

2.3 Types of UWB Transmission

The two most common methods by which a UWB signal is transmitted are the IR-UWB, and MB-OFDM UWB. In IR-UWB technology, pulses of a very short duration (usually in the order of sub-nanoseconds) are transmitted, and it is because of this property of short pulses that the signal reaches several GHz of bandwidth [8]. On the other hand, the MB-OFDM UWB combines the OFDM technique with a multi-band approach. The entire UWB spectrum is divided into sub-bands having a -10dB bandwidth of 500MHz or more. This thesis has adopted the IR-UWB transmission system. The two types of UWB transmission are explained in detail in the following subsections.

2.3.1 Impulse Radio (IR) UWB

The IR-UWB is considered to be a carrier-less transmission. Since the pulses used for transmission are in sub-nanoseconds and hence very short, the signal reaches several GHz of bandwidth and because of the narrowness of transmitted pulses, it has a fine time resolution. IR-UWB systems do not require the use of mixers, and thus low cost transmitter and receiver designs can be achieved. As explained in Section 2.2, there are several pulse shapes that can fit into the FCC's definition of UWB. One such pulse is a Gaussian monocycle pulse as shown in Figure 2-4. The transmitted power of IR-UWB can be kept low whenever the coverage area is not large. One important feature of IR-UWB is the impulsive natures of transmission, where the multiuser interference differs substantially from the continuous transmission systems and this impulsive nature of transmission allows low transmit power compared to continuous transmission systems. Fine time resolution is another important feature of IR-UWB that provides location and distancing capabilities to wireless networks.

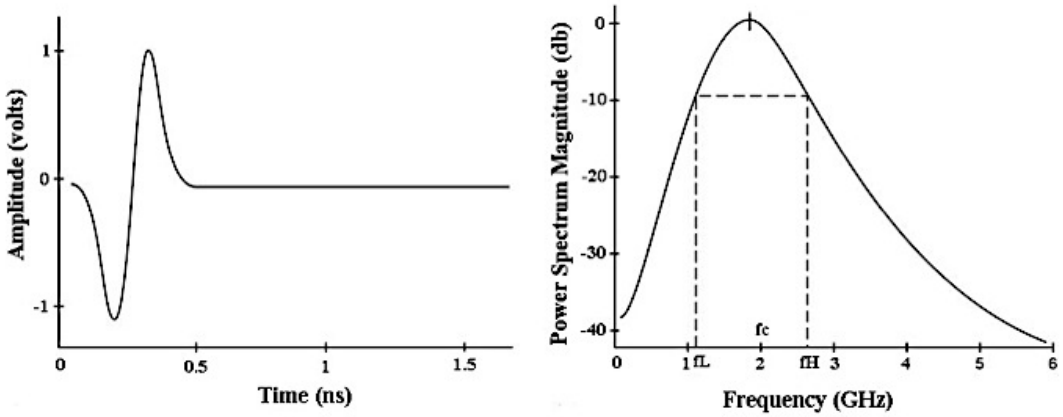

Figure 2-4 : Gaussian monocycle pulse in Time and Frequency Domain [9]

2.3.2 Multiband OFDM

In Multiband OFDM, the spectrum is divided into several sub-bands, each having bandwidth of 500MHz or more. The data that has to be transmitted is interleaved on these sub-bands and then transmitted through a multicarrier (OFDM) technique.

According to the proposal given in [10], the MB-OFDM technique is used as the physical layer for future high speed WPANs. In this proposal, the entire spectrum (3.1GHz – 10.6GHz) is divided into 14 sub-bands, with each sub-band having a bandwidth of 528MHz. These sub-bands can be added or dropped by the system depending on the interference caused or being affected by other existing wireless communication systems. In [11], a detailed band plan is given for systems using MB-OFDM, as shown in Figure 2-5. According to this band plan, in order to avoid any interference between the UWB systems and existing WPAN, only 13 bands are used. The first three lower bands are mandatory for standard operations and rest of the bands is optional or used for any future expansions.

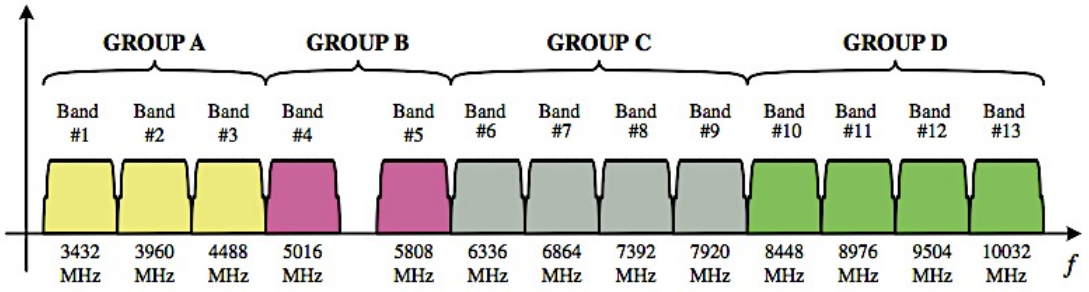

Figure 2-5 : MB-OFDM Frequency Band Plan [11]

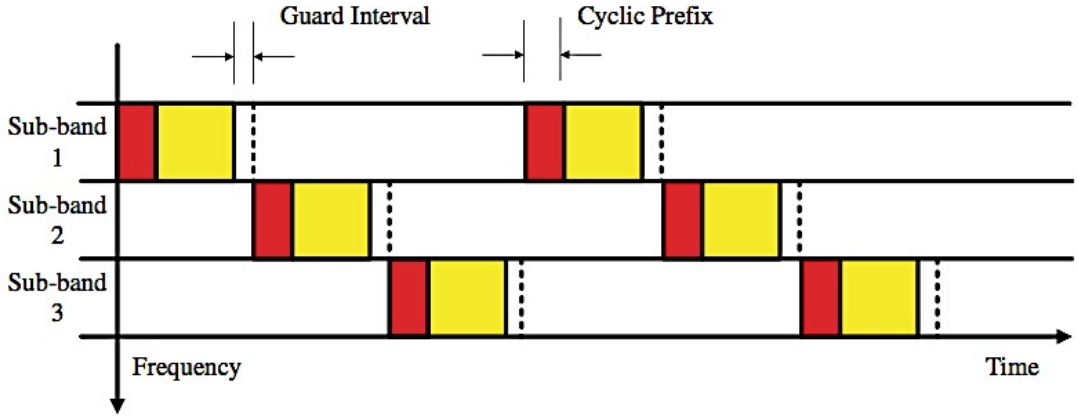

Figure 2-6 : Time-Frequency coding for MB-OFDM [12]

The MB-OFDM transceiver design uses time-frequency codes to specify center frequencies for the transmission of each OFDM symbol, and this differs from the traditional wireless OFDM systems [12]. Figure 2-6 is an example, which shows the usage of three sub-bands over the pool of 14 sub-bands for OFDM transmission. In time domain perspective, the first OFDM signal is transmitted over the first sub-band, the second symbol in the second sub-band, and so is the third symbol in the third sub-band and this repeats over time. Different time-frequency codes open the door to provide multiple accesses, where each user is assigned a unique time-frequency code.

2.4 Advantages of UWB

UWB signals have some of their own unique properties. The most important characteristic is the large bandwidth. This large bandwidth used by UWB pulses significantly increases the data rate or the channel capacity of UWB wireless communication systems. This is explained in Shannon's capacity equation below:

$$C = BW \log_2\left(1 + \frac{S}{N}\right) \tag{2.3}$$

where, C is the channel capacity, BW is the channel bandwidth, and S/N is the signal to noise ratio. From the above equation, it is evident that if either the BW or the S/N ratio increases, the channel capacity also increases, and this proves that the data rate is increased when we have a large bandwidth.

The other significant advantage of UWB is lower cost and complexity. The transceiver architecture of an IR-UWB system is so simple that it does not use any carrier used for modulation, as in the case of existing narrowband techniques.

The digital nature of UWB, combined with its operation at lower power levels, makes it a good candidate for wireless communication systems that require secure transmissions.

The nature of short duration UWB pulses, in the order of sub-nanosecond range, allows UWB to provide greater immunity against multi path losses.

2.5 Channel Characterization of UWB

Due to observations made in several channel measurements based on a clustering phenomenon in [13], an UWB channel model was proposed based on Saleh-Valenzuala [14] model with slight modifications. In [13] a Log Normal distribution was followed over the Rayleigh distribution for the multipath gain magnitude. In addition to the better

fit over the measurement data provided by Log Normal distribution, independent fading for each cluster as well as each ray within the cluster is also assumed [13]

Based on [13], the multipath model consists of the following, discrete time impulse response

$$h_i(t) = X_i \sum_{l=0}^{L} \sum_{k=0}^{K} \alpha_{k,l}^{i} \delta(t - T_l^i - \tau_{k,l}^i) \tag{2.4}$$

where $\alpha_{k,l}^{i}$ are the multipath gain coefficients, T_l^i is the delay of the l^{th} cluster, $\tau_{k,l}^{i}$ is the delay of the k^{th} multipath component relative to the l^{th} cluster arrival time T_l^i, X_i represents the log-normal shadowing, and i refers to the i^{th} realization.

By definition, we have $\tau_{0,l} = 0$. The distribution of cluster arrival time and the ray arrival time are given by

$$\begin{aligned} p\left(T_l \middle| T_{l-1}\right) &= \Lambda \exp\left[-\Lambda\left(T_l - T_{l-1}\right)\right], \quad l > 0 \\ p\left(\tau_{k,l} \middle| \tau_{(k-1),l}\right) &= \lambda \exp\left[-\lambda\left(\tau_{k,l} - \tau_{(k-1),l}\right)\right], \quad k > 0 \end{aligned} \tag{2.5}$$

where,

Λ = cluster arrival rate;

λ = ray arrival rate, i.e., the arrival rate of path within each cluster.

The channel coefficients are defined as follows:

$$\alpha_{k,l} = p_{k,l} \xi_l \beta_{k,l},$$

$$20\log 10(\xi_l \beta_{k,l}) \propto \text{Normal}(\mu_{k,l}, \sigma_1^2 + \sigma_2^2), \tag{2.6}$$

or

$$\left|\xi_l \beta_{k,l}\right| = 10^{(\mu_{k,l}+n_1+n_2)/20} \tag{2.7}$$

where $n_1 \propto \text{Normal}(0,\sigma_1^2)$ and $n_2 \propto \text{Normal}(0,\sigma_2^2)$ are independent and correspond to the fading on each cluster and ray, respectively,

$$E\left[\left|\xi_l \beta_{k,l}\right|^2\right] = \Omega_0 e^{-T_l/\Gamma} e^{-\tau_{k,l}/\gamma}, \tag{2.8}$$

Here, T_l is the excess delay of bin l and Ω_0 is the mean energy of the first path of the first cluster, and $p_{k,l}$ is equiprobable +/-1 to account for signal inversion due to reflections. The $\mu_{k,l}$ is given by

$$\mu_{k,l} = \frac{10\ln(\Omega_0) - 10T_l/\Gamma - 10\tau_{k,l}/\gamma}{\ln(10)} - \frac{(\sigma_1^2+\sigma_2^2)\ln(10)}{20} \tag{2.9}$$

In the above equations, ξ_l reflects the fading associated with the l^{th} cluster, and $\beta_{k,l}$ corresponds to the fading associated with the k^{th} ray of the l^{th} cluster. Note that a complex tap model (used to measure channel coefficients) was not adopted here. The complex baseband model is a natural fit for narrowband systems to capture channel behavior independently of carrier frequency, but this motivates to use a real-valued simulation at RF for UWB systems.

Finally, since the lognormal shadowing of the total multipath energy is captured by the term, X_i, the total energy contained in the terms $\alpha_{k,l}^i$ is normalized to unity for each realization. This shadowing term is characterized by the following:

$$20\log 10(X_i) \propto \text{Normal}(0,\sigma_x^2) \tag{2.10}$$

On summary, there are 7 key parameters involved in describing this channel model:

Λ = cluster arrival rate;

λ = ray arrival rate, i.e., the arrival rate of path within each cluster;

Γ = cluster decay factor;

γ = ray decay factor;

σ_1 = standard deviation of cluster lognormal fading term (dB).

σ_2 = standard deviation of ray lognormal fading term (dB).

σ_x = standard deviation of lognormal shadowing term for total multipath realization (dB).

These parameters are extracted from a channel response. Since it is not easy to extract all possible channel characteristics, the alternative characteristics that are used to derive the above model parameters can be the following:

- Mean excess delay
- RMS delay spread
- Number of multipath components (defined as the number of multipath arrivals that are within 10 dB of the peak multipath arrival)
- Power decay profile

Through careful studies of experimental results, there are four different channel models as proposed by IEEE 802.15 working group for WPAN.

Channel Model 1 (CM1): This is based on Line Of Sight (LOS) having a range of (0-4m) channel measurements.

Channel Model 2 (CM2): This is based on Non-Line Of Sight (NLOS) having a range of (0-4m) channel measurements.

Channel Model 3 (CM3): This is based NLOS having a range of (4-10m) channel measurements.

Channel Model 4 (CM4): This model was generated to fit a 25-nanosecond RMS delay spread representing an extreme NLOS multipath channel.

For all the above channel models, a sampling time of 167psec was considered. From [13], the following table lists some initial model parameters for a couple of different channel characteristics that were found through measurement data:

Table 2-2 : The IEEE 802.15 UWB Channel Characteristics [13]

Model Parameters	**CM 1**	**CM 2**	**CM 3**	**CM 4**
Λ (1/nsec)	0.0233	0.4	0.0667	0.0667
λ (1/nsec)	2.5	0.5	2.1	2.1
Γ	7.1	5.5	14.00	24.00
γ	4.3	6.7	7.9	12
σ_1 (dB)	3.3941	3.3941	3.3941	3.3941
σ_2 (dB)	3.3941	3.3941	3.3941	3.3941
σ_x (dB)	3	3	3	3
Model Characteristics				
Mean excess delay (nsec) (τ_m)	5.0	9.9	15.9	30.1
RMS delay (nsec) (τ_{rms})	5	8	15	25
NP_{10dB}	12.5	15.3	24.9	41.2
NP (85%)	20.8	33.9	64.7	123.3
Channel energy mean (dB)	-0.4	-0.5	0.0	0.3
Channel energy std (dB)	2.9	3.1	3.1	2.7

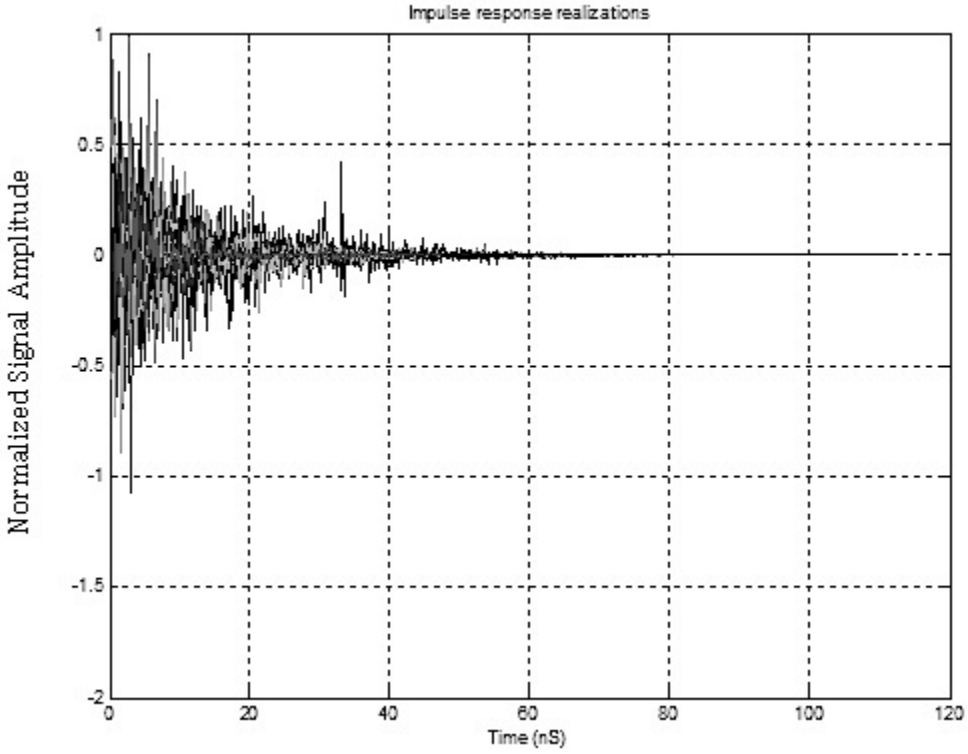

Figure 2-7 : Channel Impulse Response of CM1 model

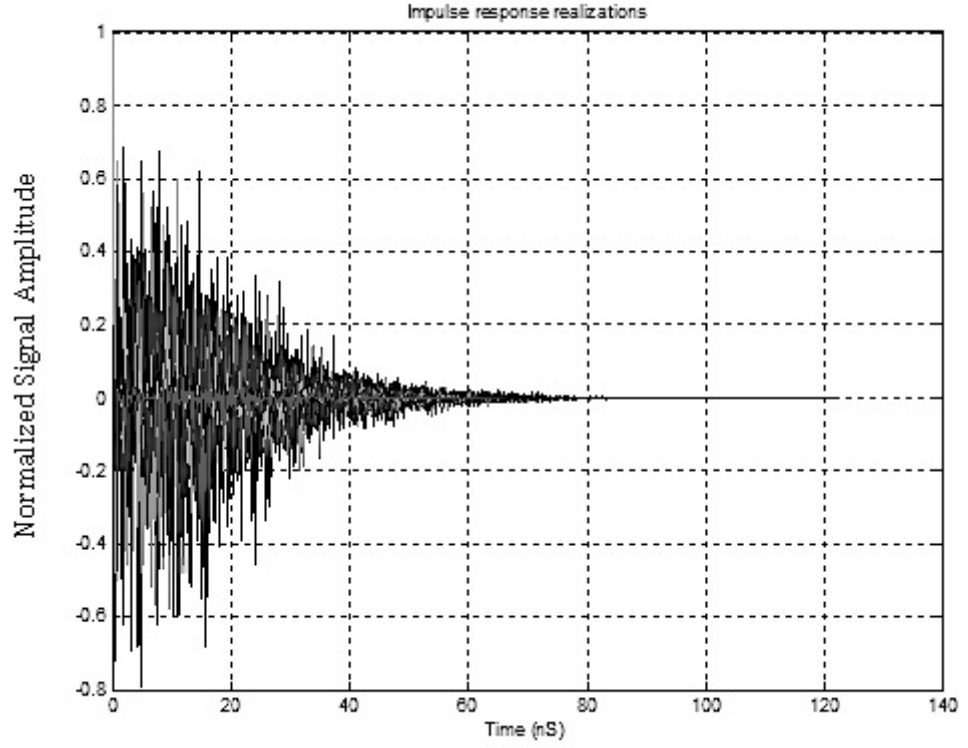

Figure 2-8 : Channel Impulse Response of CM2 model

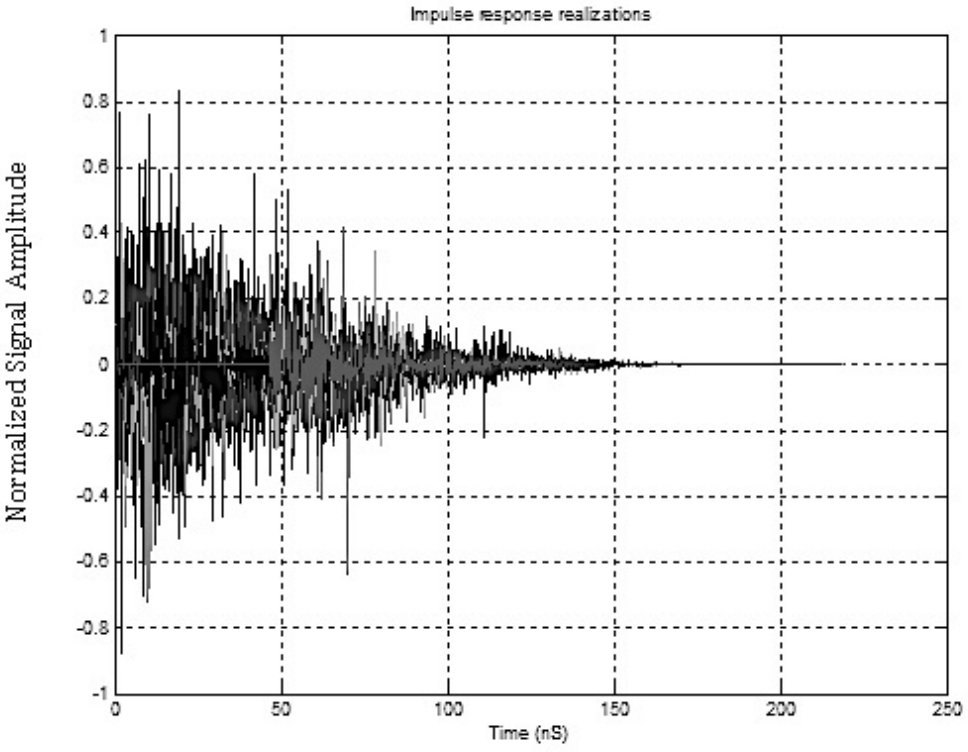

Figure 2-9 : Channel Impulse Response of CM3 model

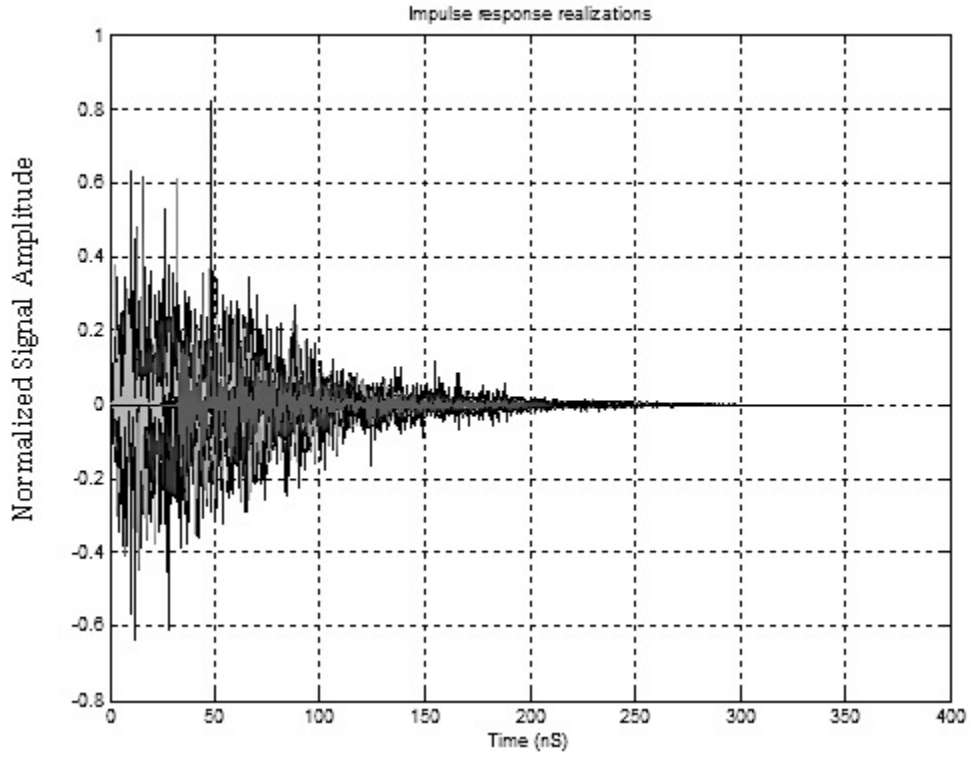

Figure 2-10 : Channel Impulse Response of CM4 model

The channel impulse responses for all of the four different channel models [13] are shown above. By observing Figure 2-6, one can notice that the multi-path delay spread varies from 90ns-120ns. For CM2, in Figure 2-7, the delay spread is just above 120ns. From Figure 2-8, for the CM3 model, this value varies between 200ns-250ns and for CM4 in Figure 2-9, the multi-path delay spread is just above 350ns.

CHAPTER 3: IMPLEMENTATION SCHEMES FOR IR-UWB

One of the biggest challenges in implementation of UWB technology is to have a suitable receiver design. In literature, there has been extensive methods addressing this problem and effective receiver structures have been developed. They are described below.

3.1 Rake Receiver

Rake receiver or All Rake receiver (A-Rake) is the optimal receiver designed for multipath channels. A UWB channel may contain a large number of multi-path components (MPC's), especially in non line of sight (NLOS) environments. Different paths experience different fading effects and a diversity technique to capture all the different paths having different fades is well exploited in a Rake receiver. The name 'Rake' comes from the garden rake fingers used to constitute the resolvable paths.

Multipath can be approximated as a linear combination of differently delayed echoes and this Rake receiver design combats the effects of multipath by detecting each echoes with a correlation finger and finally adding those detected echoes algebraically. A number of correlators connected in parallel and operating in a synchronous fashion constitute the Rake receiver design and is shown in Figure 3-1. There are basically two inputs given to each correlator: a delayed version of the received signal and a replica of the pseudo-noise (PN) sequence used as the spreading code to generate the spread spectrum modulated signal at the transmitter. This PN sequence thus acts as a reference signal.

The branches shown in the Figure 3.1 above are called as Rake branches and the received signal is multiplied to the estimated channel coefficients in each Rake branch tuned to each resolvable path.

The channel coefficient estimates are considered to be the conjugate of the actual coefficient of the actual path in order for the receiver to deliver an optimum performance.

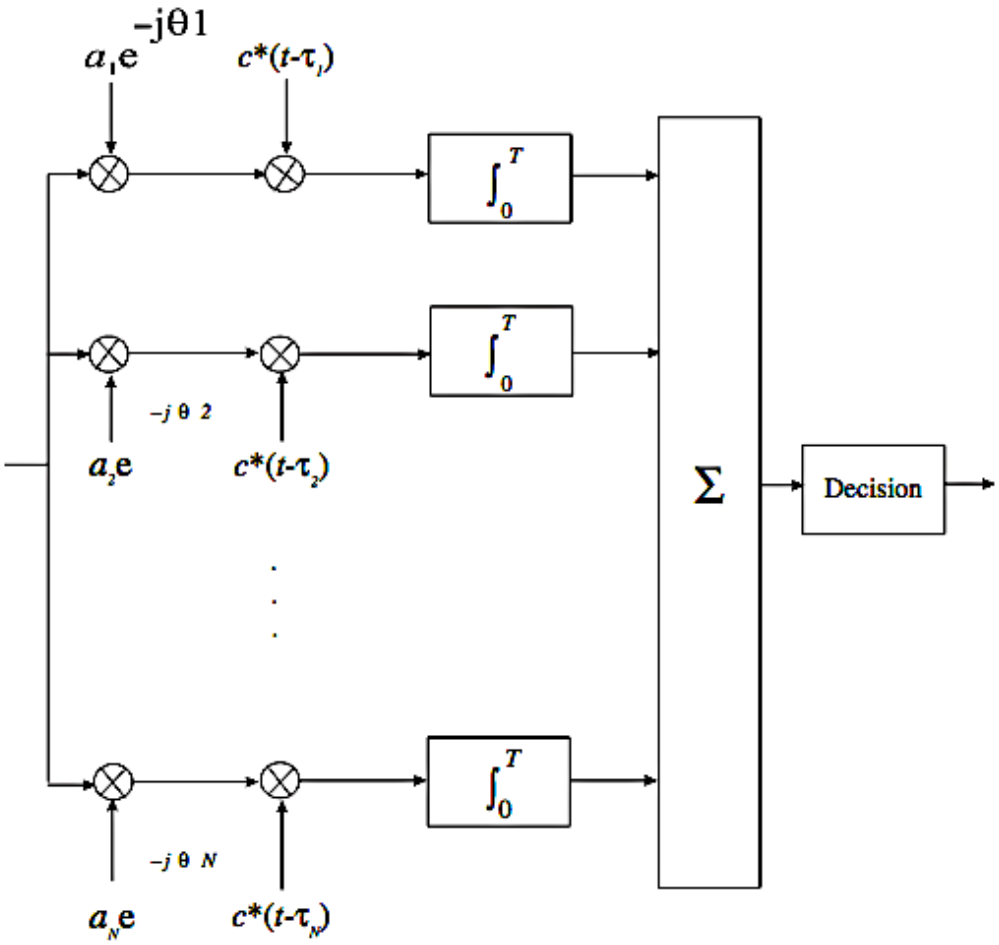

Figure 3-1 : General Rake Receiver Structure [1]

Further modifications were made to the Rake receiver structure where the MPC's with the strongest energies are selected and combined together. This type of selective combination applied to a Rake receiver is called as the Selective Rake receiver (S-Rake) and is far less complex than the A-Rake receiver, where S-Rake receiver requires less correlation fingers due to reduced number of MPC's that has to be captured. A brief detailed comparison on how the MPC's are collected using both the receiver types is

explained in the Figure 3-2 below. However, the reduced complexity of S-Rake receiver has a direct trade off with performance [15]. In Figure 3-2, L represents the number of MPC's combined by the receiver. As seen in the Figure 3-2, the A-Rake receiver collects all the MPC's, while the S-Rake receiver collects the MPC's only with the strongest energies, and in this case L=7.

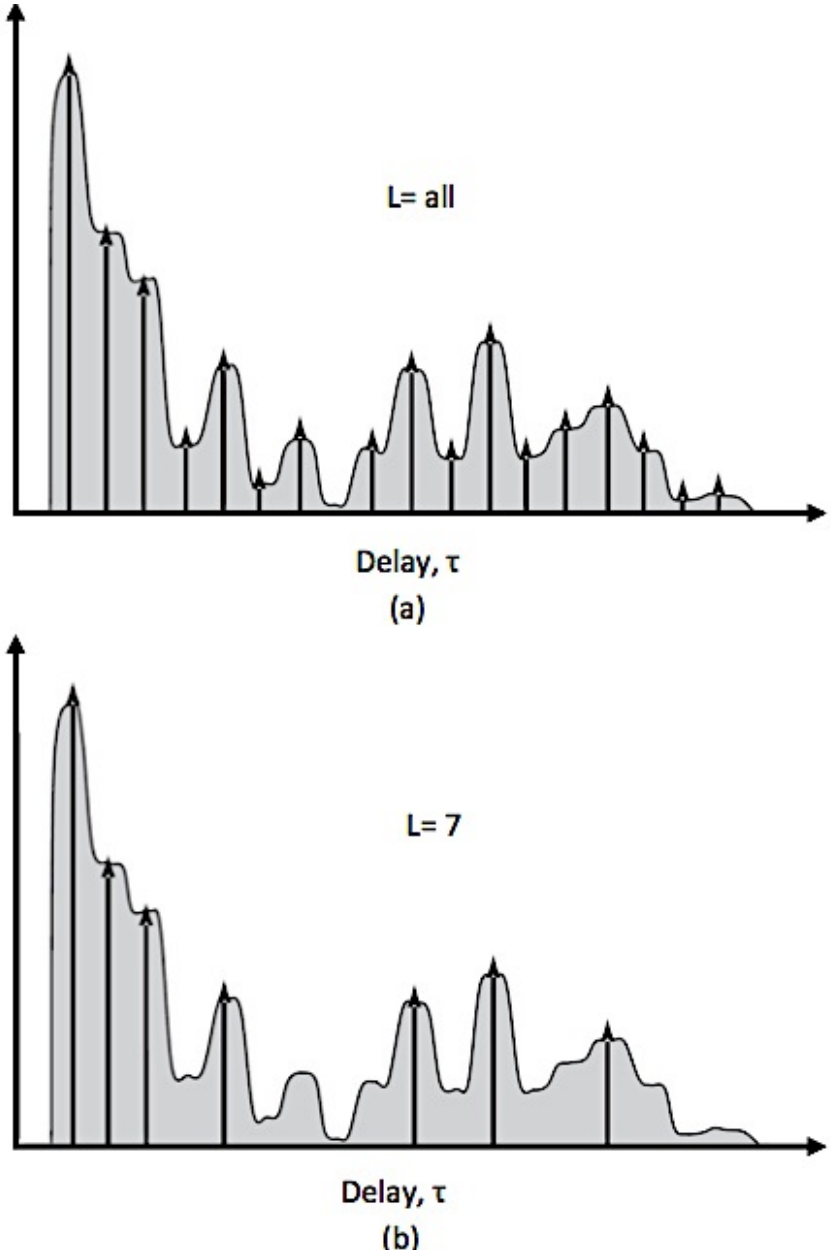

Figure 3-2 : MPC acquisition of the (a) A-Rake and (b) S-Rake Receivers

In summary, by increasing the number of diversity paths, a better performance can be achieved using a Rake receiver. Thus the Rake receiver helps for an enhanced detection of UWB signals in multipath wireless channels.

As explained in Chapter 2, one of the main drawbacks of UWB signal is its vulnerability to multipath effects. Many Rake fingers will be required to capture energy due to the extremely large bandwidth characteristics of the UWB signals. The more the number of Rake fingers required, the more would be the system complexity. The other big drawback of this receiver design is that the distortion of the pulse shape. Each multipath goes through different channels having different fading effects and this directly affects the distortion of the pulse shape, which makes use of a single LOS path signal as a template suboptimal [16].

3.2 Transmit Reference (TR) Receiver

As explained in Section 3.1, the Rake receiver becomes complex when there are many resolvable paths; the number of amplitudes and delays that has to be calculated becomes large. Also, high sampling rates are required to perform channel estimation.

In order to avoid the computational complexity related to channel estimation, a transmitted reference (TR) receiver is introduced [17]. In this TR receiver each data pulse is preceded with an un-modulated reference pulse (also known as pilot pulse) separated by a delay D, known to the transmitter and receiver. The transmission follows a frame pattern, where each frame has duration T_f, and in this frame duration the reference pulse is transmitted followed by the data pulse. These two pulses are assumed to go through same level of distortion and multipath fading as long as the delay between these two pulses are kept below the channel coherence time. (The channel coherence time is the minimum time before the channel gets uncorrelated with its previous state) [18][19].

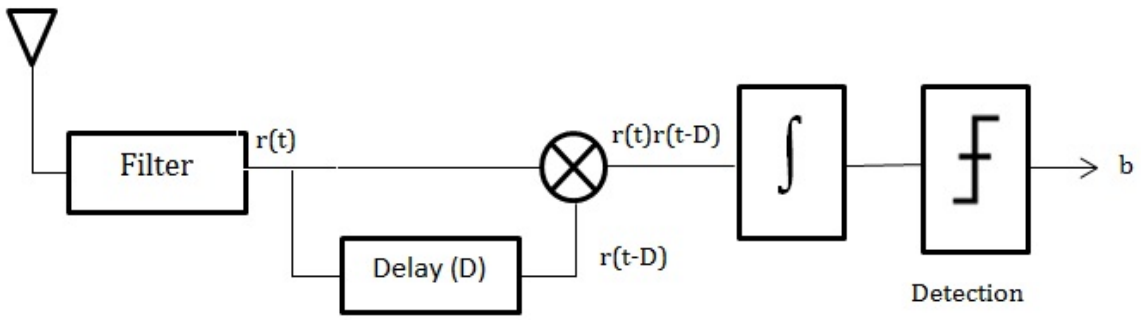

Figure 3-3 : General TR receiver structure [20]

A general receiver structure for TR receiver is shown in Figure 3-3. In order to recover the transmitted signal, the data is detected by correlating the received signal with the received reference pulse with a delay. By this method, the reference pulse is used as a perfect template to extract the data pulse. The detection process is shown in Figure 3-4.

In this method, since the reference and data pulse are transmitted through the same channel, the reference pulse acts as a preamble for its following data pulse, thereby providing good synchronization. Furthermore, for a UWB system demanding low power consumption, this TR receiver gives the ability to capture significant energy from the received signal due to multipath components by correlating the received signal with its reference pulse.

Despite having significant advantages, the TR receiver has few drawbacks. Hardware realizations become complex, as this method requires the UWB delay element to be incorporated, which is hard to fabricate in DC integrated circuits. Also, the performance of this receiver is fairly poor for low Signal-to-Noise Ratio (SNR) values or in the presence of narrowband interference [21]. Another major setback for this method is that, half of the transmitted waveform is used as pilot reference and this eventually reduces the transmission rate and efficiency.

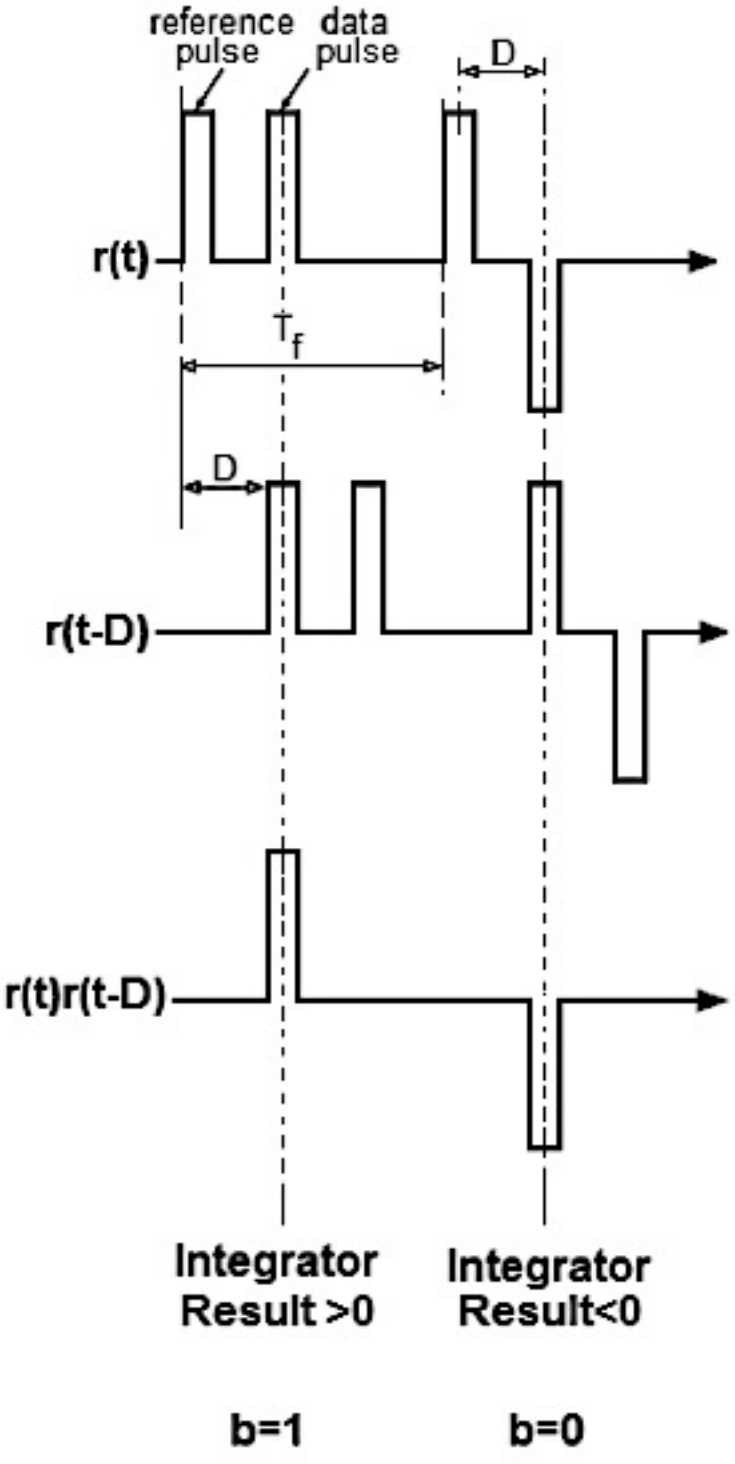

Figure 3-4 : Example of T-R receiver demodulation procedure [22]

3.4 Frequency Shifted Reference (FSR) Receiver

Alternatively, a slight frequency shifted technique was then developed to overcome the effects of time domain separation between the reference and data pulse used by T-R technique. Instead of shifting those two pulses in time, the pulses are shifted in frequency and this results in avoiding the delay element at the FSR receiver [20] [23]. Contrasting the FSR receiver with T-R receiver, in T-R method both the reference and data pulses must undergo the same fading and the delay time between the two pulses should be significantly smaller than the channel coherence time as explained in Section 3.2, whereas in FSR receiver this particular parameter is the frequency offset present between the reference pulse and data pulse, and this offset should be smaller than the coherent bandwidth of the channel [23].

For low-data rate applications, of a bit rate of less than 100 kb/s, the frequency shift should be well below the frequency coherence of the channel so that this frequency shift provides the reference pulse to act as a perfect template for the data bearing signal. According to [23], the transmission scheme for this method deals with frames per symbols and is given by the equation:

$$T_s = N_f T_f \tag{3.1}$$

where, T_s is the symbol duration and N_f is the number of pulses present in one frame and T_f is the frame duration. The transmission can be carried out by sending one reference pulse followed by a data pulse or a series of data pulses each separated by a frequency offset. The orthogonality between the reference and data pulse is looked upon in the entire symbol period rather than at frame-by-frame period,

$$f_{offset} = \frac{1}{N_f T_f} = \frac{1}{T_s} \tag{3.2}$$

The general structure of FSR-UWB receiver is shown in Figure 3-5. This structure uses only one data sequence having the same frequency offset, used in shifting data sequences before transmission. This offset provides a shift to the reference signal and this helps in providing a perfect template to extract the useful information from the data pulse sequences.

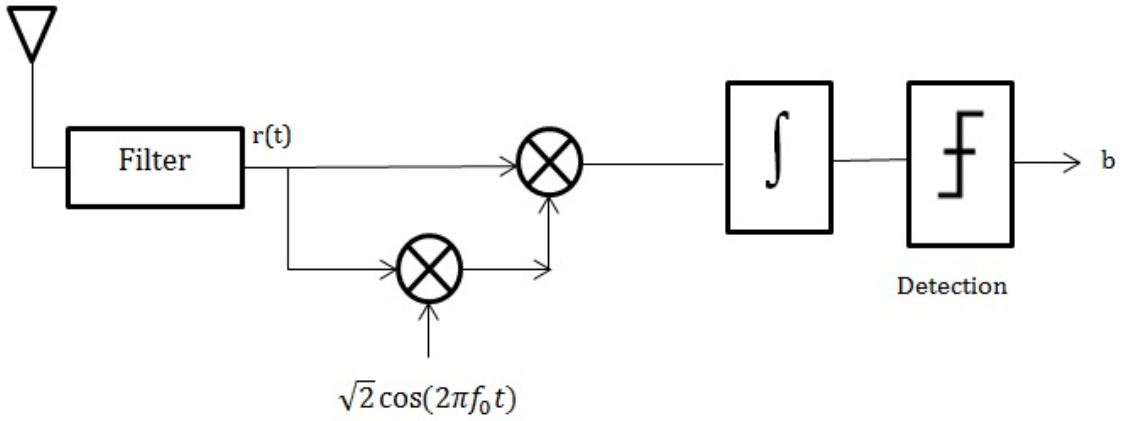

Figure 3-5 : FSR-UWB receiver structure [23]

Overcoming the drawbacks of delay line used in TR-UWB receiver, FSR receiver has its own drawbacks. The implementation complexity of FSR-UWB system is relatively high due to employment of analog carriers that are used to shift the IR-UWB signals. Moreover, the frequency offsets affects the performance due to oscillator mismatch, phase offsets caused by multipath fading, and amplitude offsets caused by nonlinear amplifier [24].

3.5 Energy Detection Receiver

In the previous sections, the three possible receiver structures for IR-UWB were discussed and it was observed that coherent receivers, TR and FSR receivers were employed, the first type having a difficult task to estimate the channel involving complex signal processing algorithms and having very high sampling rates [25] [26], while in the

TR case, analog delay lines are very difficult to implement and also their attenuations are prohibitive for delays exceeding few tens of nanoseconds [27]. The FSR on the other hand, employs analog carriers for shifting of IR-UWB signals and increases system complexity [24].

Alternatively, Energy Detection Receivers (EDRs) outperformed the RAKE and T-R receiver structures in terms of simplicity and performance. EDRs combined with binary pulse position modulation (PPM) proved to be effective and easier to implement [28].

3.5.1 Pulse Position Modulation (PPM)

In nominal pulse position, where the encoding of data is carried out with two or more positions of pulses in time forms the principle of pulse position modulation.

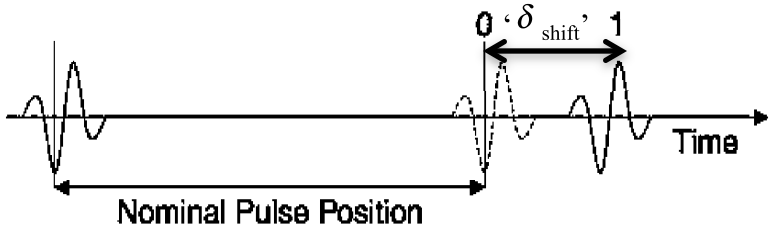

Figure 3-6 : Pulse Position Modulation

As shown in Figure 3-6, the pattern followed is a two-position modulation (2PPM) in which each data is represented by an impulse and if the pulse is present at the nominal pulse position then it is interpreted as bit '0' and if a pulse is present after the nominal pulse position, then it is interpreted as bit '1'. Additional positions can also be added to accommodate more bits per symbol. In ideal cases, the time separation between nominal pulses would be greater so as to avoid interference issues, and the time delay (*d*) between the pulses would be in the range of nanoseconds (ns). The delay *d* is carefully selected in such a way that, it is greater than the maximum channel delay spread in order to avoid any ISI and also to maintain orthogonality between the received pulses.

3.5.2 Energy Detection Receiver with PPM

With binary pulse position modulation (BPPM) employed using an energy detecting receiver structure, bit '0' is transmitted in the first half of the symbol period and bit '1' is transmitted in the second half of the symbol period. The nominal pulse period T_s determines a BPPM frame. Each frame contains one transmit pulse. Depending on the BPPM symbol value, the pulse is present at either the first or second BPPM half-frame of duration $T_s/2$. At the receiver side, signal energies are calculated for each half frame of the symbol period and then these two energies are compared against each other to determine the position of the transmitted pulse in either of the half frame having highest signal energy. Implementation of EDRs require much lower sampling rates compared to the coherent receivers and involves simple components in terms of circuit complexity [29].

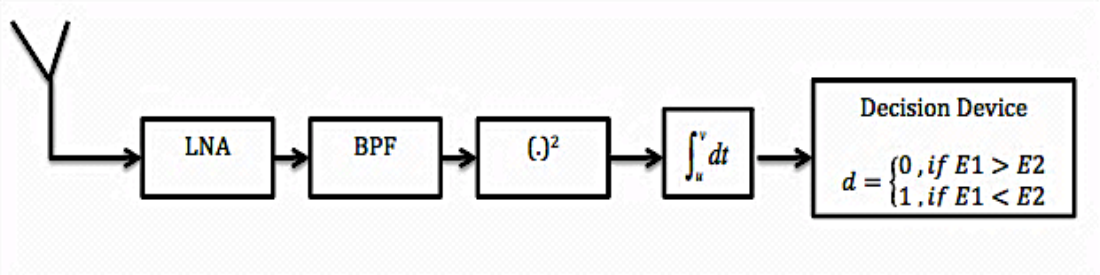

Figure 3-7 : Energy Detection Receiver with PPM

At the transmitter side, the data to be transmitted is modulated according to the equation as follows [30]:

$$s(t) = \sum_j p[t - jT_s - (1 + b_j)\delta / 2] \tag{3.3}$$

where, $p(t)$ is the UWB pulse with duration of T_p, with a frequency range varying from f_L to f_H. T_s is the symbol duration and δ is a time constant. In Figure 3-7, the received signal is squared before it is passed to an integrator and this squaring operation can be

implemented by using a simple square law device such as Schottky diode operating in its square region. The integration is performed for each half frame or each time slot, from $[jT_s, jT_s + T_M]$ and $[jT_s + \delta, jT_s + \delta + T_M]$. The decision device is then operated based on energy present on both the half frames of a symbol period. Or, in simple words, the energy present in both the time slots is compared with each other. Detection of UWB signals is shown in the following equations:

$$r_{j0} = \int_{jT_s}^{jT_s+T_M} r^2(t)dt \tag{3.4}$$

$$r_{j1} = \int_{jT_s+\delta}^{jT_s+T_M+\delta} r^2(t)dt \tag{3.5}$$

where, *r(t)* is the received signal, r_{j0} and r_{j1} are the energies present during the first and second slot of a symbol period. The value T_M varies from T_p for an additive white Gaussian noise (AWGN) channel to δ in a dense multipath channel with severe delay spread. The decision device uses the following decision rule to detect the information bits.

$$bj = \text{sgn}(r_{j1} - r_{j0}) \tag{3.6}$$

3.6 Comparisons of Three types of Transceivers:

In [34] the BER of the TR transceiver under multipath channels has been derived as:

$$BER_{TR} = Q\left(\frac{\alpha E_b}{\sqrt{2\alpha E_b N_o + 2N_o^2(f_H - f_L)T_M}}\right) \tag{3.7}$$

where the TR transceiver transmits one information bit over two pulses. From [20] and [23], the BER of FSR transceiver under AWGN channel has been derived as:

$$BER_{FSR} = Q\left(\frac{\sqrt{M}E_b}{\sqrt{(2M+1/2)E_bN_o + N_fN_o^2(f_H - f_L)T_f}}\right) \tag{3.8}$$

In [12], the BER of ED-PPM under multipath channels has been derived as:

$$BER_{ED-PPM} = Q\left(\frac{\alpha E_b}{\sqrt{2\alpha E_bN_o + 2N_o^2(f_H - f_L)T_M}}\right) \tag{3.9}$$

M is the information bits that are simultaneously transmitted through N_f UWB pulses for the FSR transceiver. It is clearly evident from equations 3.7 to 3.9 that the BER of TR and ED-PPM fare better than the FSR transceiver. Again, the BER of TR and ED-PPM are exactly the same and they perform well over the FSR transceiver. Although the performances of TR and ED-PPM are the same, the complexity of the system is very less in the latter case. The absence of delay element in ED-PPM transceiver makes them a suitable candidate for low power and low complex IR-UWB systems.

Comparing ED-PPM with FSR, due to the delay spread of multipath channels, the analog carriers in the received IR-UWB have multiple phases, but the analog carriers reproduced by the FSR transceiver have only one phase. Consequently multipath errors arise and this has an impact on the amount of signal energy collected by the FSR receiver. Therefore, the BER performance for FSR under multipath channels will be still lower than that given by equation 3.8, which is under AWGN channel. Because, there are no analog carriers used by the ED-PPM transceiver, it does not suffer from multipath errors.

The rest of this thesis concentrates on ED-PPM transceiver, and their BER characteristics are exploited under ISI conditions in the next chapter.

CHAPTER 4: INTERSYMBOL INTERFERENCE AND SIGNAL PROCESSING METHODS

4.1 Intersymbol Interference

ISI occurs as a result of frequency selective fading, where a received signal over the symbol period experiences interference from adjacent symbols due to delay effects caused by multipath propagation. Depending on when the pulse is sampled, the receiver can make incorrect decision, causing bit errors. ISI can also be described as the superposition of time-shifted smeared pulses. This is explained in Figure 4-1. ISI contributes to an irreducible error floor that is totally independent of signal power. This error floor is difficult to analyze since it depends on ISI characteristics such as channel properties and sequence of transmitted symbols and also on the modulation type being involved in the system.

In [31] Bello and Nelin carried out an extensive analysis of ISI degradation to symbol error probability by assuming a Gaussian delay profile for the channel with cases involving only the adjacent symbols leading to ISI. The expressions used in the analysis were still complex as they were totally dependent on channel delay profile and transmission characteristics. By treating ISI as uncorrelated White Gaussian in [32], an approximation to symbol error probability was obtained. Several researches indicate that the pulse shapes used in UWB significantly impacts the irreducible error floor. Moreover, the irreducible error floor is more sensitive to the root mean square (RMS) delay spread of the channel than the shape of the channel power delay profile.

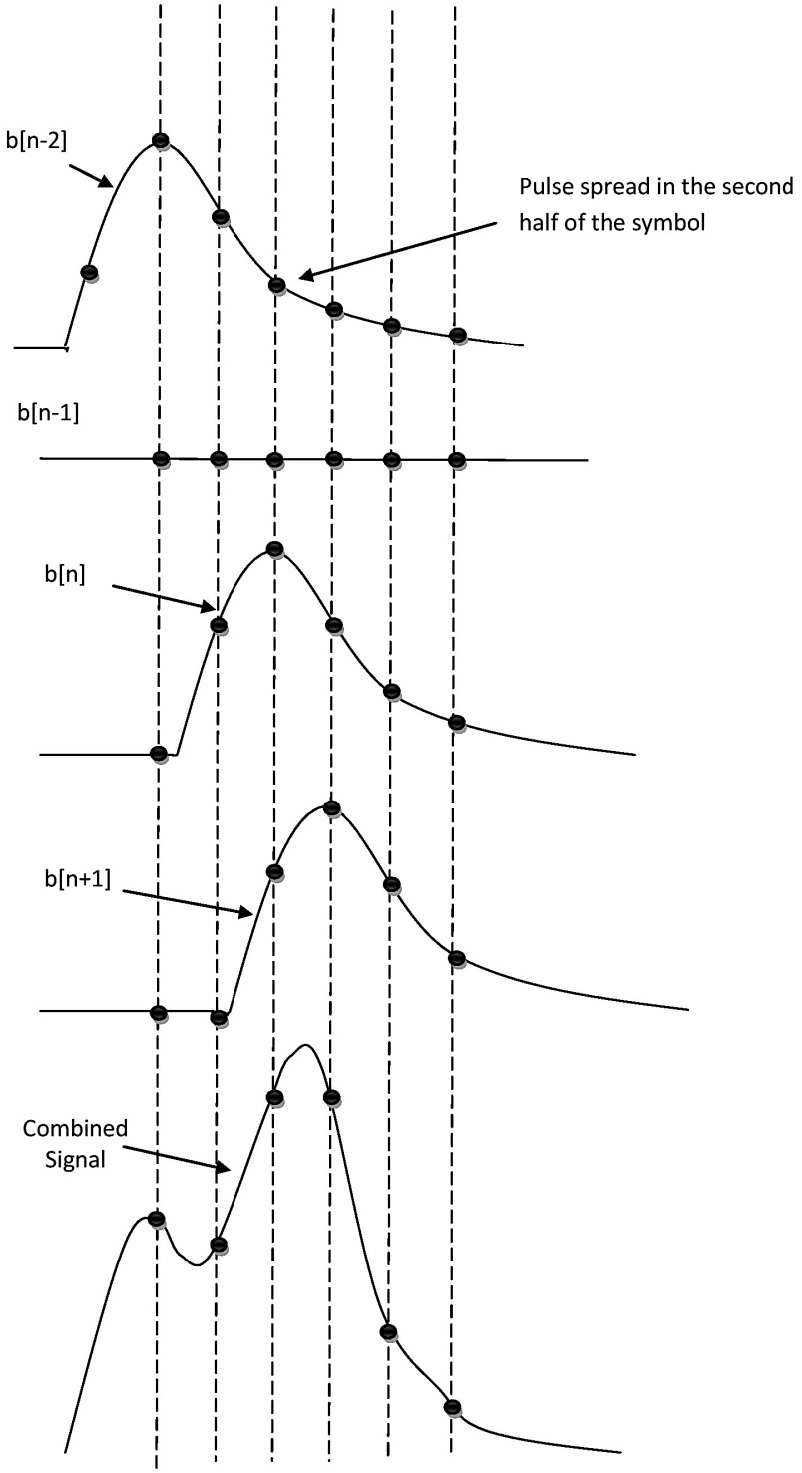

Figure 4-1 : Illustration of ISI as a result of channel maximum excess delay

4.2 Equalization

From Section 4.1, it was clear that the channel delay spread plays a vital role in causing ISI and hence contributes to an irreducible error floor. Several techniques were proposed in the past in order to mitigate the effects of ISI. Equalization is one such technique employing signal processing methods at the receiver side to alleviate the effects of ISI. Equalization can also be implemented at the transmitting side, but receiver implementation is most common given the diversity of the channel. Delay spread control measures can also be provided through antenna solution. Due to the limited scope of this thesis, we concentrate only on signal processing techniques employed at receiver level.

When RMS delay spread is greater than the channel symbol time, an irreducible error floor is formed. Digital communications involving high data rate applications usually require high performance equalizers. Mitigating the effects of delay spread is considered one of the major hurdles in designing a high data rate digital communication system. Whenever a good equalizer is designed, a balance has to be maintained by not enhancing the noise power in the received signal, in the process of mitigating ISI. Noise power enhancement is a common problem in equalizer design; hence, a good equalizer design should not enhance the noise power in the received signal.

Linear equalizers suffer more from noise enhancement than the non-linear equalizers, but the later has higher complexity. Moreover, the equalizer should adapt itself to fluctuating channel conditions by understanding the channel impulse so as to reduce the effects of ISI. Serving the above purpose, generally training pulses are used to measure the channel impulse response.

Equalization techniques can be broadly classified into two types: linear and non-linear. Figure 4-2 summarizes the equalizer types that are available in literature.

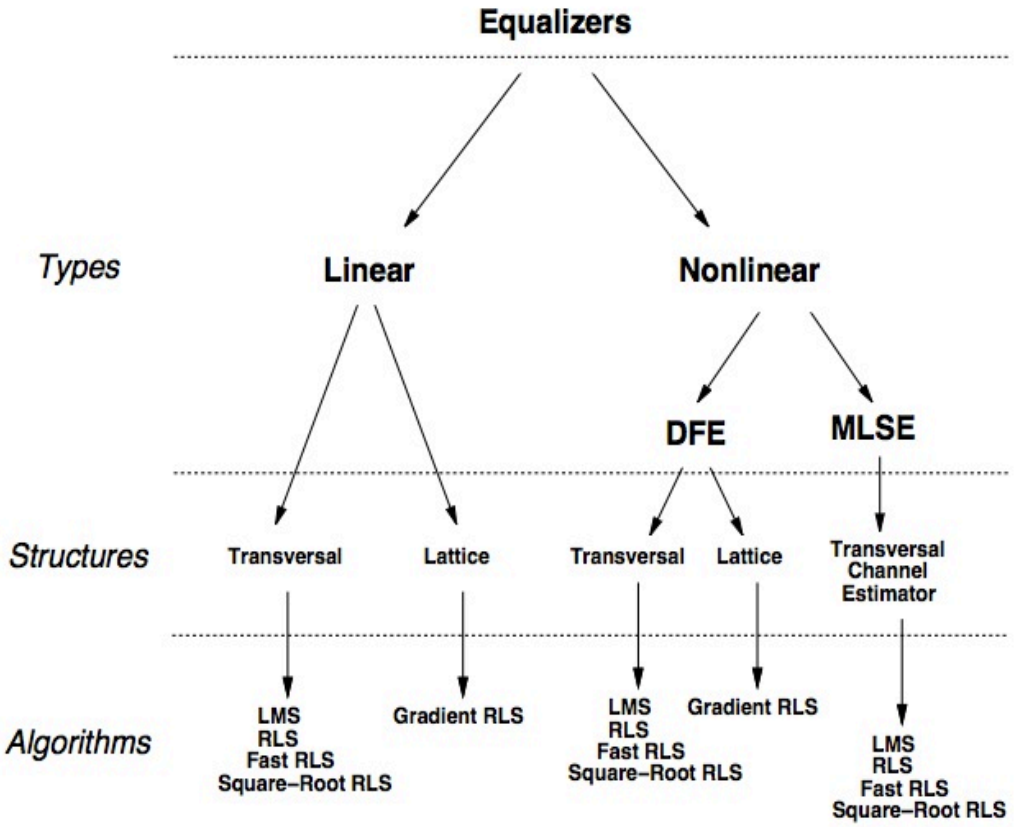

LMS: Least Mean Squares
RLS: Recursive Least Squares
DFE: Decision Feedback Equalization
MLSE: Maximum Likelihood Sequence Estimation

Figure 4-2 : Classification of Equalizers

Among the equalizer types, linear equalizers suffer from noise enhancement or frequency selective fading and are, therefore not used in wireless communication systems. Equalizers can also be classified as symbol-by-symbol (SBS) detectors or sequence estimators (SE). All linear equalizers as well as Decision Feedback Equalizers (DFE) belong to the SBS category where ISI is eliminated at symbol level by detecting each symbol individually. On the other hand, SE equalizers detect sequences of symbols, so the effect of ISI is a part of the estimation process. Maximum likelihood sequence estimation (MLSE) belongs to this category and is an optimal equalization technique. The

main drawback with MLSE is that the complexity grows exponentially with increase in channel memory length.

In the following sections, some of the commonly used equalizations are discussed in detail.

4.3 Linear Equalizers

Linear equalization can be implemented by using a simple linear transversal filter or by means of a zero forcing equalizer. The filter structure has a computational complexity that is directly proportional to the channel dispersion length L. The output of the demodulator is directly given to the transversal filter as shown in Figure 4-3, and the resulting output is the estimate of information sequence.

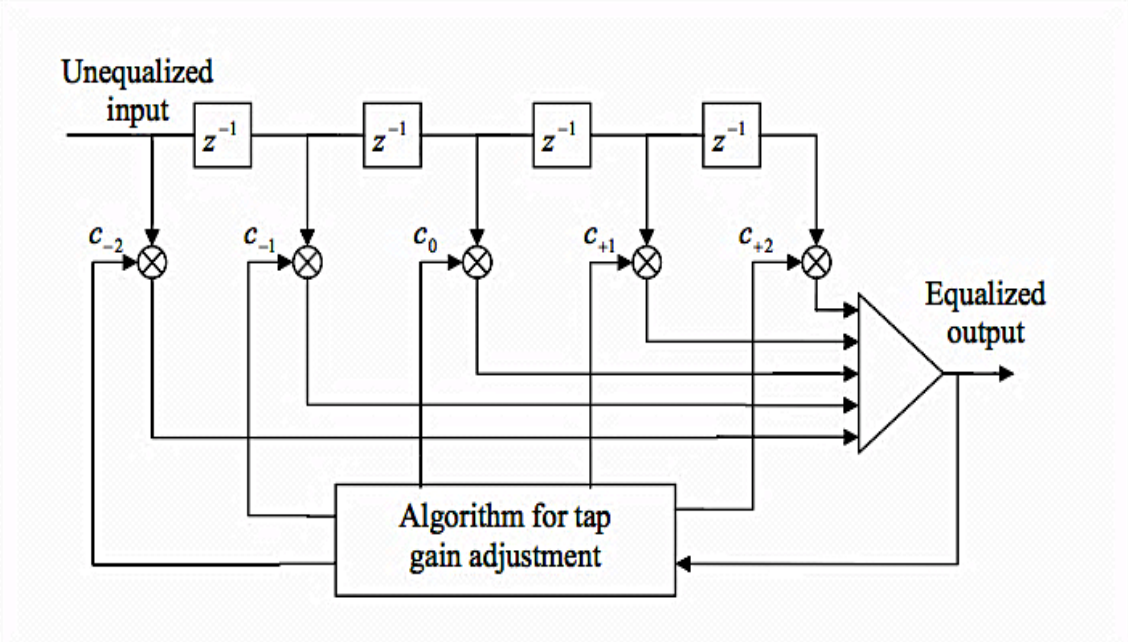

Figure 4-3 : Linear Transversal Equalizer [33]

The values of c_j are complex valued tap coefficients of the transversal filter. Careful selection of coefficients is followed in order to minimize the average probability error.

Two main equalizers are used in determining the tap coefficients of transversal filter. They are the peak distortion and the mean-square error equalizers.

4.3.1 Peak Distortion Equalizer

If an equalizer employs just a simple inverse filter to an equivalent discrete time model of the channel response having infinite number of taps, ISI can be completely eliminated and this filter is called as the zero-forcing equalizer. In this equalizer, an inverse of the channel frequency response is applied to the received signal in order to restore the properties of the transmitted signal. In ideal conditions, when the channel is noiseless, zero-forcing equalizer will remove most or all ISI.

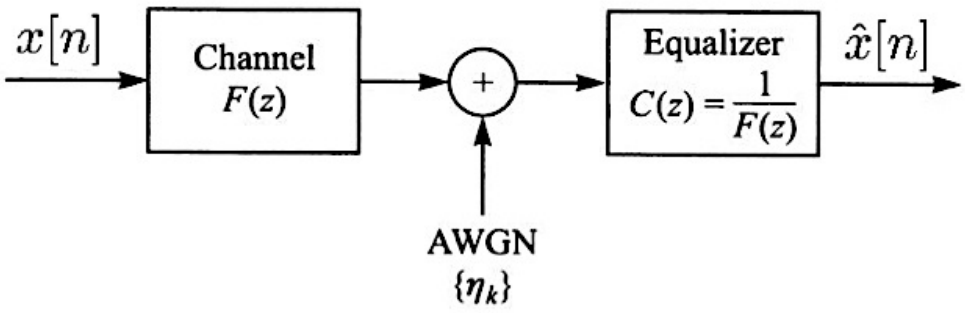

Figure 4-4 : Block Diagram of channel with Zero-Forcing Equalizer [33]

A detailed block diagram of the channel with zero-forcing equalizer is shown in Figure 4-4. An in-depth analysis of this equalizer is out of scope of this thesis, but can be found in [33].

The peak distortion criterion has a convex function over the tap coefficients and this distortion can be minimized in carrying out a numerical analysis by applying the method of deepest descent [33].

4.3.2 Mean Square Error (MSE) Linear Equalizer

According to [33], in MSE criterion, the tap coefficients are modified in such a way to minimize the mean square value of error.

$$J = E\left|\varepsilon_k\right|^2 = E\left|I_k - \hat{I}_k\right|^2 \tag{4.1}$$

where I_k is the information symbol transmitted in the kth signaling interval, and $\hat{I}_k$ is the estimate at the output of the equalizer. J is a quadratic function of the equalizer coefficients. This quadratic function yields a set of linear equations by minimizing J with respect to the equalizer coefficients. In contrast, an orthogonal principle used in mean square estimation can be used to obtain the linear equations. The principle of orthogonality can be stated as, "The necessary and sufficient condition for the cost function J to obtain its minimum value is for the corresponding value of the estimation error ε_k to be orthogonal to each input sample that enters into the estimation of the desired response at time k." Therefore, the tap weight can be obtained by solving this set of linear equations.

4.4 Decision Feedback Equalization (DFE)

Similar to the linear equalizers, DFE has a feed-forward filter, which receives sequence as its input followed by a feedback filter having previously detected sequence as its input. The feedback filter plays a vital role in eliminating ISI based on previously detected symbols. The ISI information present in the previously detected symbols is stored as coefficients of the feedback filter and this value is subtracted from the next incoming symbol. The DFE structure is shown in Figure 4-5. The feedback *D(z)* filter present in the loop, must be strictly causal otherwise the system becomes unstable.

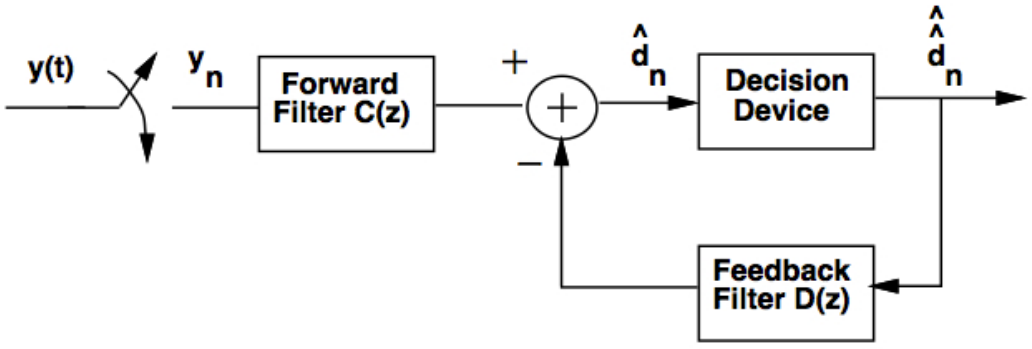

Figure 4-5 : Decision Feedback Equalizer structure [33]

DFE estimates the channel frequency response and not its inverse, and hence DFE does not suffer from noise enhancement. DFE performs well with channels having deep spectral nulls compared to the linear equalizers. The feedback filter contains only the previously detected symbols; hence the equalizer is no longer a linear model. The filter tap coefficients can be found by either using LMS or any adaptive algorithms or by just using training sequence to measure the leaking energy of the previously detected symbol that can be used as a subtraction coefficient.

All these simple features make this equalizer perfect in mitigating ISI in impulse radio Ultra-Wideband communications. DFE combined with the simple energy detector employing PPM discussed in Chapter 3, gives rise to a simple and effective solution to cancel the effects of ISI. Two new algorithms are proposed in Chapter 5, having this simple solution improve the performance of a basic energy detector using PPM.

CHAPTER 5: SIGNAL PROCESSING IN RECEIVERS: PROPOSED SCHEMES AND COMPARISONS

The limitation of high data rates that an IR-UWB receiver could handle was discussed in Chapter 4. In this chapter, the performance of the energy detector receiver using PPM under weak ISI and strong ISI conditions are discussed. A new scheme is proposed to improve the performance of ED-PPM and a couple of alternative approaches to combat ISI are examined. A detailed performance comparison is then given on all of the approaches at the end of this chapter.

5.1 Performance of ED-PPM under ISI

As discussed in Chapter 2, the channel impulse response (CIR) of the CM1 model varies between 80ns-150ns. In order to provide sufficient time for the pulse in the CM1 channel to die out completely before the occurrence of the next pulse, careful selection of the pulse repetition period (T_f) has to be considered. Since the CIR of the CM1 channel varies from 80ns-150ns, the pulse repetition period should be greater than or equal to 80ns at least in order to prevent any pulse overlaps or energy leakage into subsequent slots.

In the case of ED-PPM employing binary pulse position modulation, has two slots for transmission of each bit. The slot period (δ) is set as 80ns and hence the bit period (T_b) becomes 160ns. This is the "No ISI" condition.

In order to study the performance of the ED-PPM transceiver under the No ISI condition, Monte Carlo simulations have been used to examine the BER of the above receiver under CM1 channel conditions. The system parameters of the computer simulations are set as follows:

a) The bandwidth of the UWB pulse (f_H-f_L) is 500MHz, with a center frequency of 3.95GHz.
b) Values for T_f and δ are set as 160ns and 80ns respectively.

c) Set the integration time $T_m = \delta$.

According to the analysis in [12], when no ISI is present, the BER of the ED-PPM transceiver under sense multipath channels is given by:

$$BER_{ED-PPM} = Q\left(\frac{\alpha E_b}{\sqrt{2\alpha E_b N_o + 2N_o^2 (f_H - f_L) T_M}}\right) \tag{5.1}$$

where $\alpha \in (0,1]$ is a constant monotonously increasing with T_m. In [30], there has been extensive investigation on the effects of T_m on the BER performance of the ED-PPM transceiver.

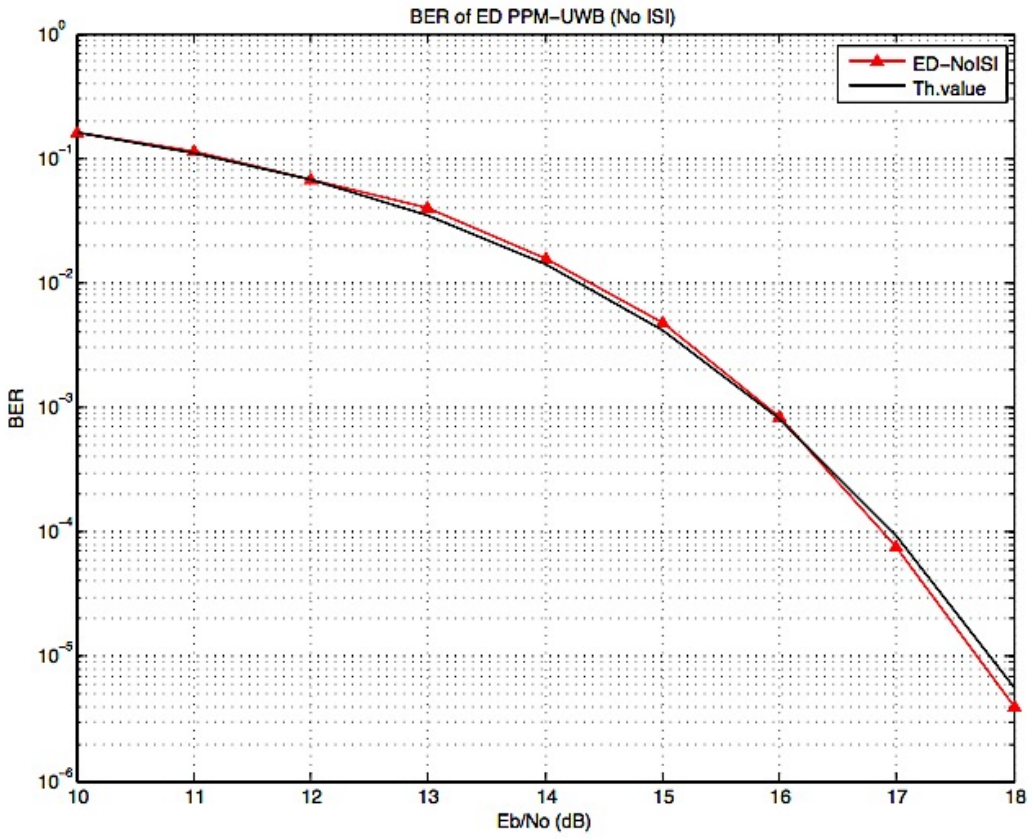

Figure 5-1 : BER performance of ED-PPM under no transmit ISI condition

From the above figure, when $T_m = \delta$, it is clearly evident that the simulation results match well with the theoretical analysis results.

5.1.1 Weak ISI Condition

In order to handle high data rates, the ED-PPM transceiver systems should transmit data at rapid rates. This is done by reducing the value of the pulse repetition period to a desired rate that suits the data rate of the system. From the previous section, we know that any value of δ less than 80ns will cause a certain portion of the pulse to spill over the subsequent slot and this results in ISI. For the weak ISI case, the slot duration δ is set to 60ns. This implies that there would be an energy spill of 20ns into the next subsequent slot. The simulated performance results are shown in Figure 5-2. It is quite evident that the energy detector undergoes significant performance degradation.

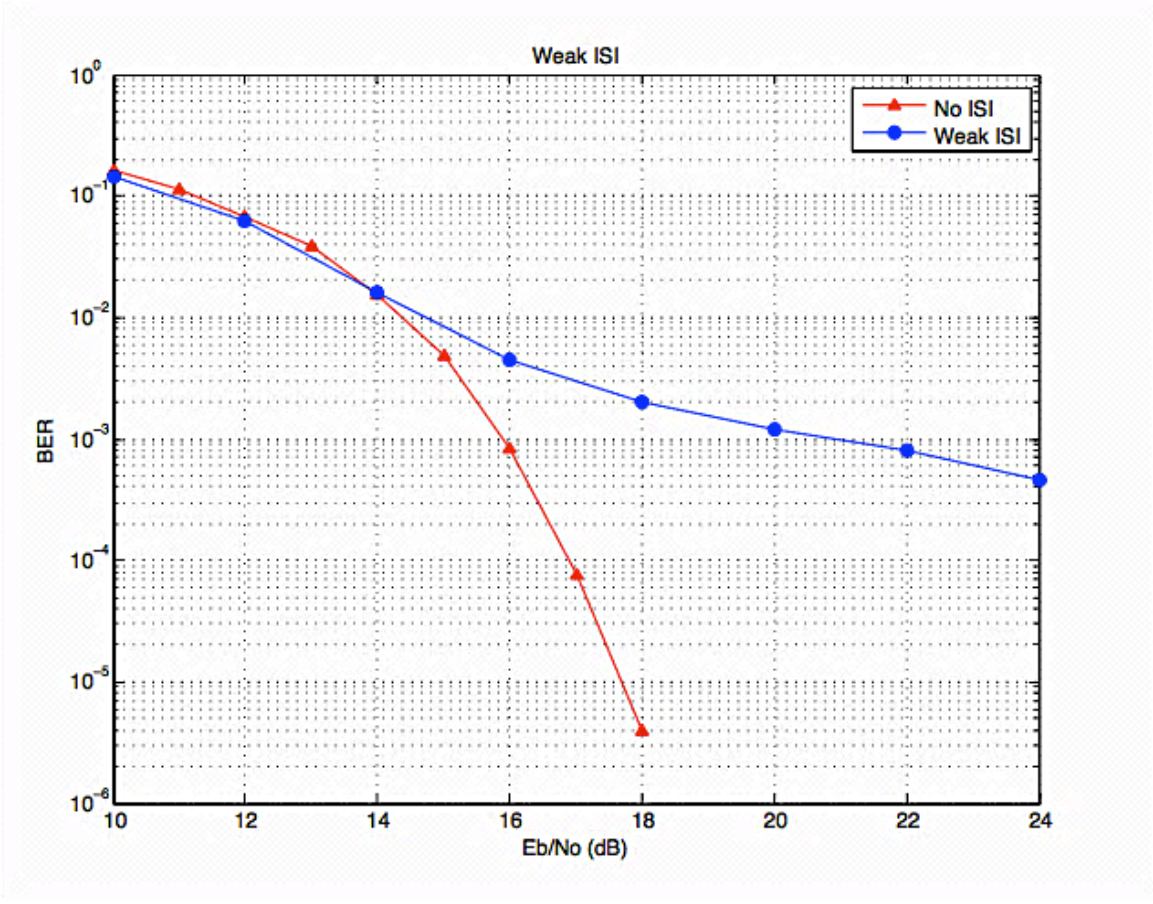

Figure 5-2 : ED-PPM Weak ISI Performance

5.1.2 Strong ISI Condition

Increase in high data rate will further increase the energy spill in the subsequent slot. For the strong ISI case, the slot duration δ is set to 30ns. Since the CIR is almost 80ns, it is clear in having a δ value of 30ns indicates that nearly half of the CIR's post-cursor elements energy would spill into the next subsequent slot. The performance of ED-PPM would further deteriorate as shown in Figure 5-3. Due to the presence of ISI, the impact of noise is not dominant over BER and reaches an error floor less than 10^{-2}.

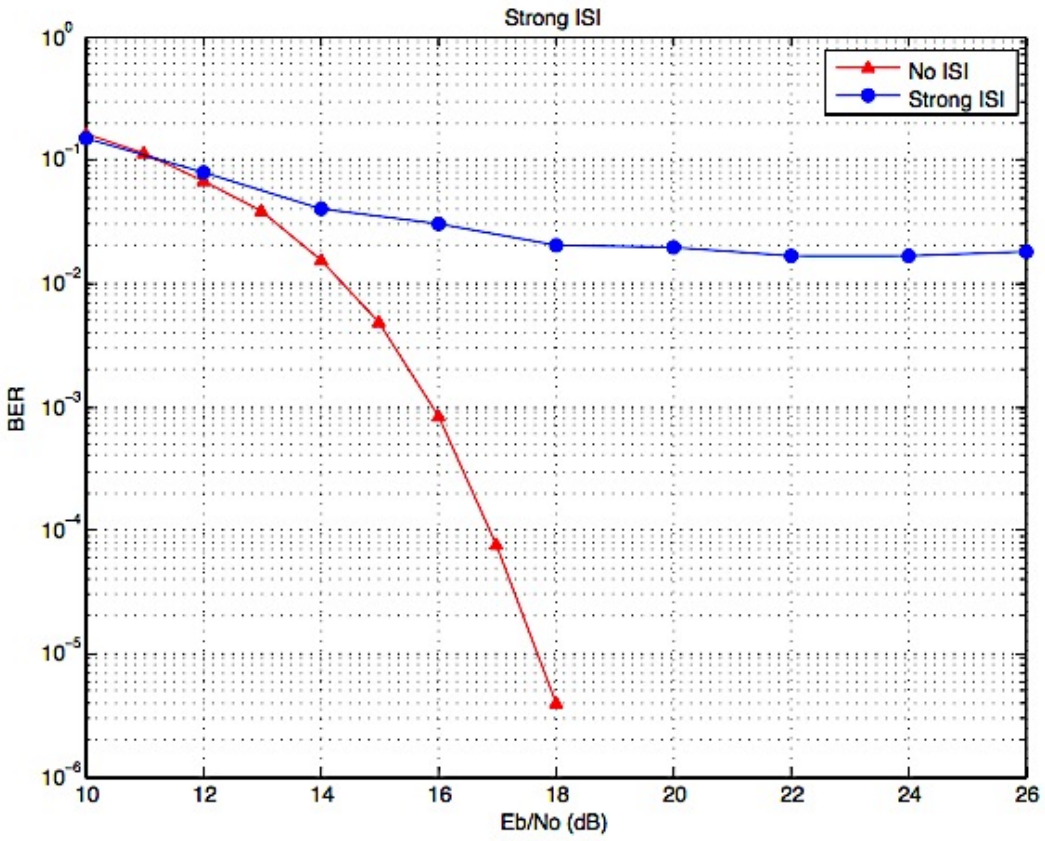

Figure 5-3 : Strong ISI Performance

5.2 ISI Mitigation: Proposed Algorithm

The ISI therefore, plays a vital role in the detection of symbols at the receiver. It is clearly shown from the above simulations that the performance of the ED-PPM

transceiver with respect to the increase in data rate affects system performance, and therefore requires an efficient signal processing at the back end, to cancel out the effects caused by ISI. T_b is directly related to the data rate of the system, and hence for higher data rates, the values of T_b should be decreased and this forces to decrease the value of δ, since δ is purely dependent on T_b.

5.2.1 Energy Subtraction Algorithm

Several traditionally available ISI elimination schemes were discussed in Chapter 4 and they all require complex computations, which further increase transceiver system complexity. Motivated by the use of decision feedback equalizers, which provides a simple and efficient way of cancelling ISI, this thesis proposes a new energy subtraction-based on pulse detection for the ED-PPM transceiver systems. As discussed in Chapter 1, the CIR of the CM1 model has only post-cursor elements and, few or no pre-cursor elements. This property makes the implementation easier, as it requires only feedback filters to cancel post-cursor elements and hence no feed-forward filters are required.

The key concept behind the energy subtraction algorithm is that, whenever a pulse is detected in a particular slot duration, the energy spill that is induced in the following slot is measured. This leakage that contributes to ISI, is then cancelled out by subtracting the stored energy subtraction coefficient with the energy present in the next incoming slot, before a decision is being made at the detector. The energy subtraction algorithm requires some key parameters to be measured. The process of finding these key parameters and the process of pulse detection with bit decision is explained in the following subsections.

In order to find the three key parameters, it is proposed to transmit a training sequence pattern sandwiched between bursts of data transmission.

5.2.1.1 Training Mode

The receiver switches to training mode at intervals sandwiched between packet data transmission. During training mode, it is assumed that the channel has non-varying conditions and hence the energy subtraction coefficients are considered to be constant for different channel paths in the CM1 model. By numerous computer simulations performed through MATLAB, it was found that the following training pattern, shown in Figure 5-4 and Figure 5-5, resulted in yielding the three key parameters required for energy subtraction.

As explained in Section 3.5.2, for data bit '0', the pulse is present in the first half of the frame, and thus the mapped training sequence becomes: [1 0 1 0 1 0 1 0 1 0]. Here, '1' represents transmission of pulse and '0' represents no pulse has been transmitted.

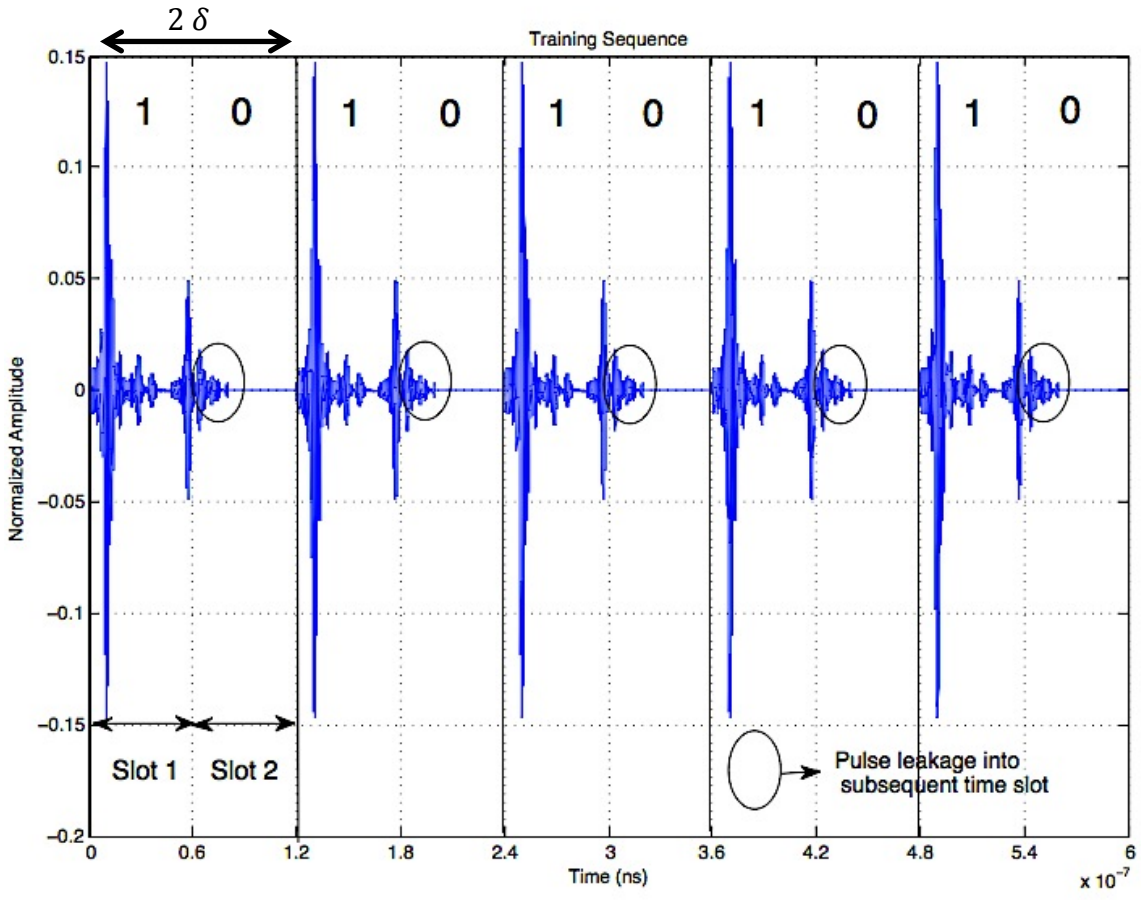

Figure 5-4 : Received Training Pulses with Weak ISI (the bit period is 2δ)

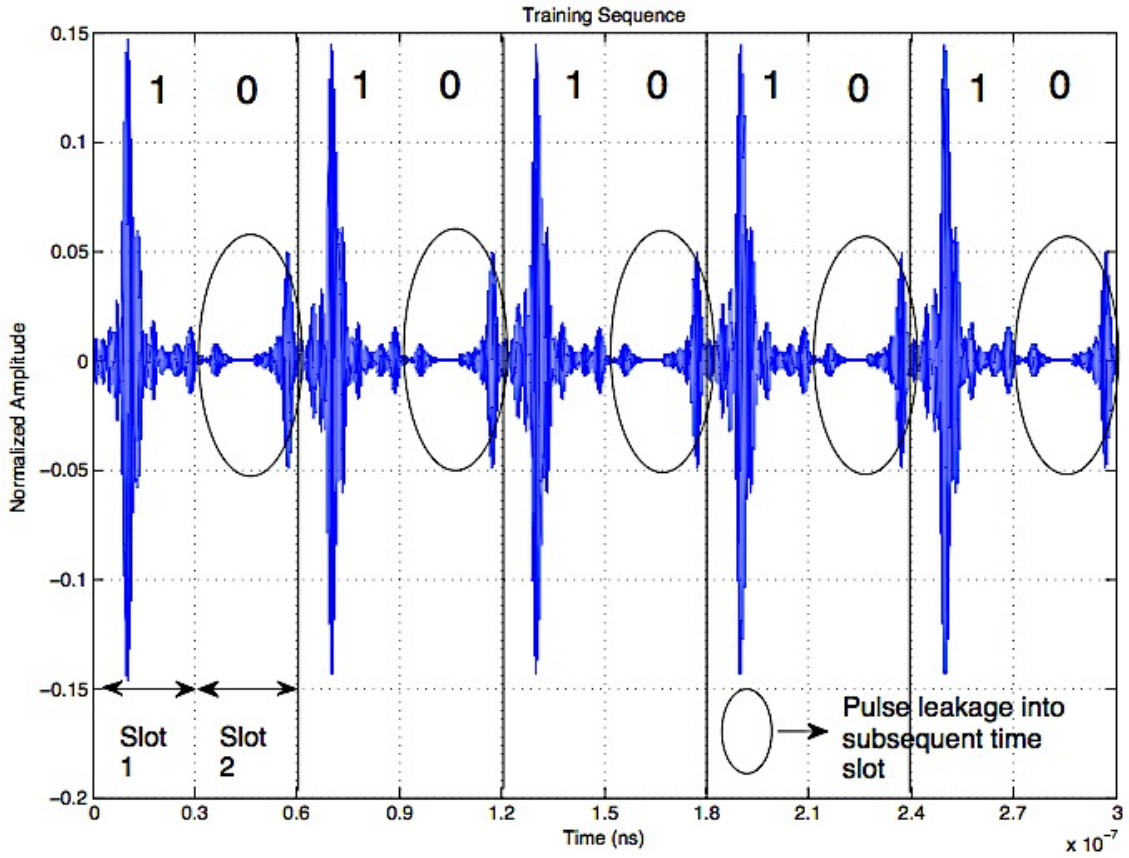

Figure 5-5 : Received Training Pulses with Strong ISI (the bit period is 2δ)

The integration time is set exactly the same as the slot duration in training mode, that is, $T_m = \delta =$ 60ns and 30ns for weak ISI and strong ISI respectively. The three key parameters that are measured from the above training pattern are:

1.) Energy Subtraction Coefficient.
2.) Energy Threshold for Pulse Detection.
3.) Noise Energy.

The training pattern from the above figures implies that, at the receiver, the energy present in the second slot of bit duration is always noise energy plus the leaking energy from the pulse in the previous slot.

Rewriting the equations from Chapter 3, when $r_L(t)$ is the received training signal,

$$r_E = \int_{jT_f}^{jT_f+T_m} r_L^2(t).dt \tag{5.2}$$

$$r_L = \int_{jT_f+\delta}^{jT_f+\delta+T_m} r_L^2(t).dt \tag{5.3}$$

where, r_E is required to measure the energy threshold for pulse detection (ε), and r_L contains leaking energy from the previous pulse plus noise energy and is therefore required to measure the energy subtraction coefficient (E_s). Here, δ is 60ns for weak ISI and 30ns for strong ISI. According to our training pattern, we need to average the r_E and r_L values to calculate ε and E_s.

$$\varepsilon = \left[\frac{\sum_{j=1}^{N} r_E}{N} \right] \tag{5.4}$$

$$r_s = \left[\frac{\sum_{j=1}^{N} r_L}{N} \right] \tag{5.5}$$

Hence, E_s can be calculated as $E_s = r_s$ – Noise Energy (N_s). The E_s value gives the energy subtraction coefficient, and this value is subtracted from the next incoming slot based on pulse detection from the previous slot. The noise energy can be simply estimated by transmitting more zeros between high pulses and measure the energy present in the 'no pulse' slot. An average of 'no pulse' slot energies from the training sequence will yield N_s. The algorithm describing how this pulse energy subtraction occurs is explained in the next section of this Chapter.

It is clearly evident that, in order to detect a pulse in a particular time slot, the energy of the pulse should be greater than the energy in the second slot; therefore, we arrive at the condition as

$$r_s < E_{TH} \leq \varepsilon \tag{5.6}$$

The E_{TH} is the threshold value required to detect a pulse and this value is picked based on the above condition.

5.2.2 ED-PPM With Energy Subtraction (ES) Algorithm based on Threshold Pulse Detection: (Proposed Heuristic Approach)

This section gives the changes in the ED-PPM transceiver block with the addition of an energy subtraction block before the decision is made. In the following subsection, the energy subtraction algorithm is explained by, how a pulse is detected and also when an energy subtraction is required.

The diagram of the ED-PPM with ES is shown below.

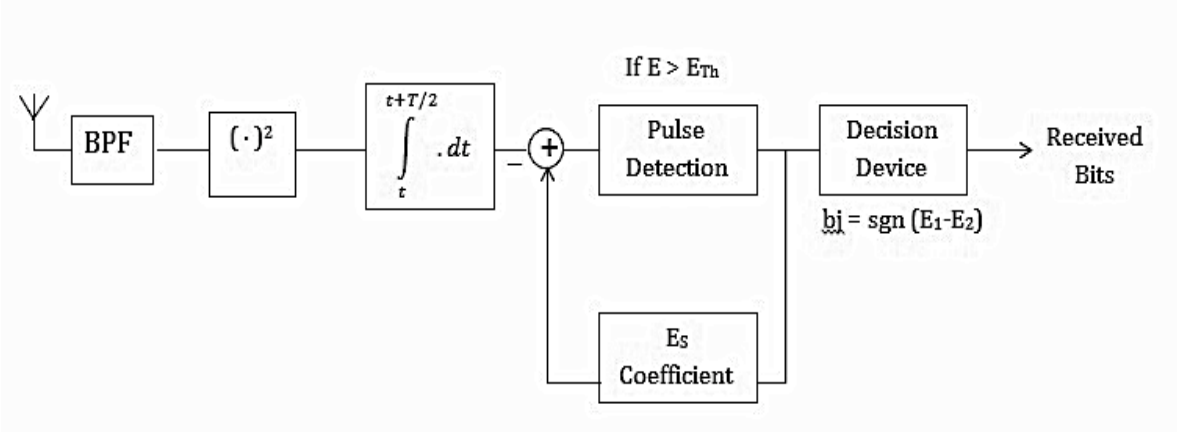

Figure 5-6 : Proposed ED-PPM Receiver with Energy Subtraction

In comparison with the ED-PPM receiver structure discussed in Chapter 3, the new model consists of a couple of new blocks implemented just before the decision device. The working concept of this transceiver is explained in the flowchart below. As explained before, the three key parameters necessary for this algorithm are found by operating the receiver in training mode, and with the help of the estimated coefficients, the energy subtraction procedure based on pulse detection is implemented wherever applicable.

The flowchart of the ED-PPM with ES is illustrated below:

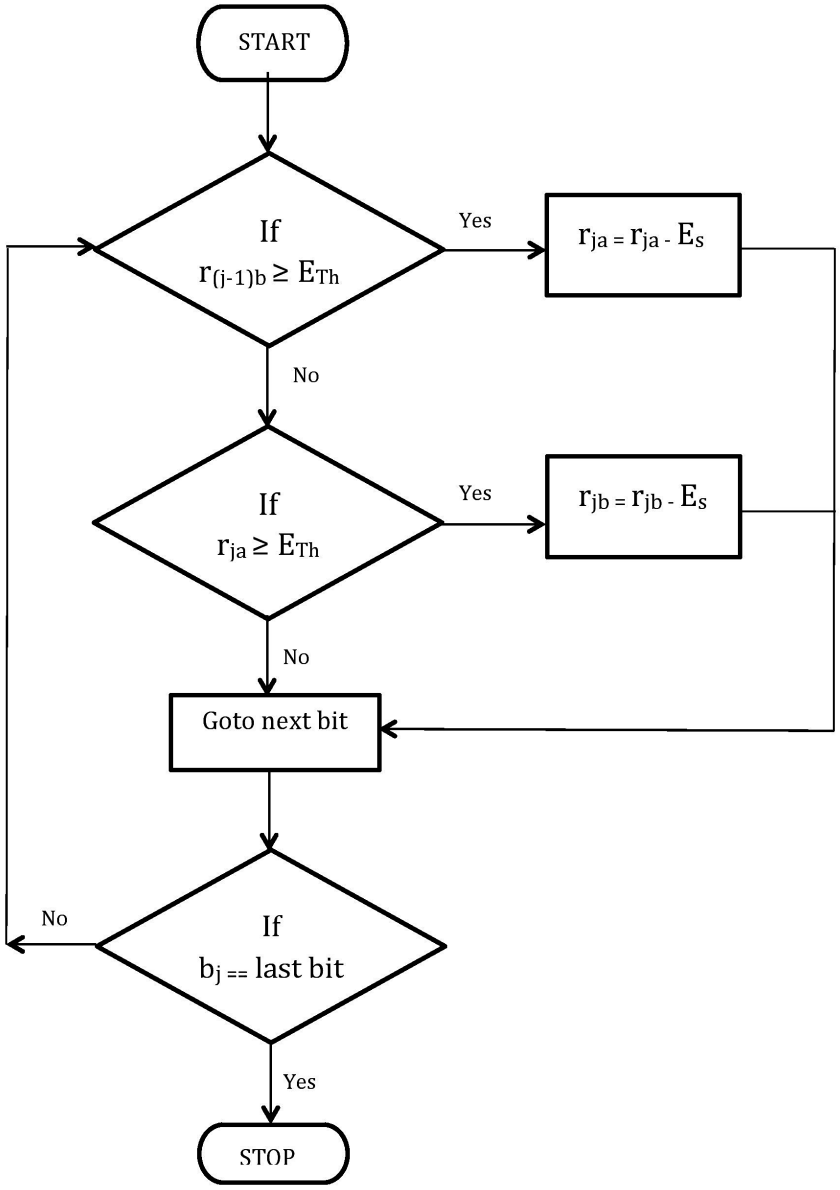

Figure 5-7 : Proposed ED-PPM with ES Flowchart

The integration time is always set to $T_m=\delta$. During data processing at the receiver, whenever a pulse is detected at a particular slot, the energy subtraction algorithm cancels

the interference caused by this pulse to the next incoming slot by subtracting the E_s coefficient with the energy present in the next incoming slot.

In the following paragraphs, the operation principle of the coefficient subtraction is described.

Let *r(t)* be the received signal integrated over the limits $[jT_f, jT_f+T_m]$ for the first slot of each bit and then from $[jT_f+\delta, jT_f+\delta+T_m]$, for the energy present in the second slot of each bit.

$$r_{ja} = \int_{jT_f}^{jT_f+T_m} r^2(t).dt \tag{5.7}$$

$$r_{jb} = \int_{jT_f+\delta}^{jT_f+\delta+T_m} r^2(t).dt \tag{5.8}$$

where, r_{ja} is the energy present in the first slot of a bit duration and r_{jb} is the energy present in the second slot of bit duration.

From the flowchart Figure 5-7, we can arrive at two explicit conditions on pulse detection, and energy subtraction is carried out based on the following conditions

$$r_{ja} = \begin{cases} r_{ja} - E_s, & if\ r_{(j-1)b} \geq E_{TH} \\ r_{ja}, & otherwise \end{cases} \tag{5.9}$$

$$r_{jb} = \begin{cases} r_{jb} - E_s, & if\ r_{ja} \geq E_{TH} \\ r_{jb}, & otherwise \end{cases} \tag{5.10}$$

Therefore, in this method, whenever a slot having energy greater than E_{TH} is detected, then the energy in the next incoming slot is subtracted from the stored energy coefficient. If the slot energy is less than E_{TH}, then no operation is performed and the pointer is

moved to the next slot. By this way, the amount of energy leaked into the subsequent slot is cancelled before a bit decision is made. Finally, the received bits which are the information bits are recovered as follows:

$$\hat{b}_j = \text{sgn}(r_{ja} - r_{jb}) \tag{5.11}$$

Simulations implementing the above algorithm were carried out, and satisfactory gain was achieved under weak and strong ISI conditions. The BER performance of the new proposed algorithm is shown and explained in the upcoming subsections where the performance of other detector is also discussed.

5.2.3 ED-PPM with ES based on Previous Bit Decisions: (Proposed Iterative Approach)

Although the above approach seemed to have mitigated ISI to an extent, it was noticed that there was a problem introduced by the threshold detector into the bit decision. Whenever the noise energy is greater than the pulse energy, it will be wrongly detected as a pulse present in that slot and hence unnecessary subtraction occurs in the next slot. From Figures 5-12 and 5-13, it is clearly evident that the problem of ISI is cancelled out to a certain extent in the previous model, but at the same time it is not as efficient as it was predicted by the design criteria.

In order to overcome these difficulties, it was necessary to arrive at a unique solution. Here, the concept of threshold detection is completely removed from the detector unit and now an iterative procedure is used for performing bit decisions. The energy subtraction algorithm, now works, based on the previously detected bits.

Recalling from Section 3.5.2, if bit ‘0’ is transmitted, ideally the pulse is present only in the first slot, and the second slot is left vacant. So, even in a strong ISI scenario, the pulse

spreads into the second slot but not to the other frame: hence it is declared that there is no ISI caused by bit '0'. On the other hand, if bit'1' is transmitted where the pulse is present in the second slot and first slot is left vacant, considering a strong ISI scenario, the pulse spreads into the first slot of the next frame. If the next frame were carrying bit '0', there would be an addition of leaking energy to the pulse energy already present in that slot. Since this is just an addition of leaking energy, there will be no significant problems caused by this type of ISI. But if the next frame is carrying bit'1', then this leaking energy fills up the empty first slot of bit'1' frame, and whenever a bit decision is made, the leaking energy is sometimes greater than the original pulse energy in the other slot. Hence bit '1' is wrongly detected as bit '0'. This model is thus designed to serve as a mitigating receiver for this type of ISI, which is the most dominating one of all ISI types that deteriorates the performance of the energy detector.

The following receiver structure is proposed:

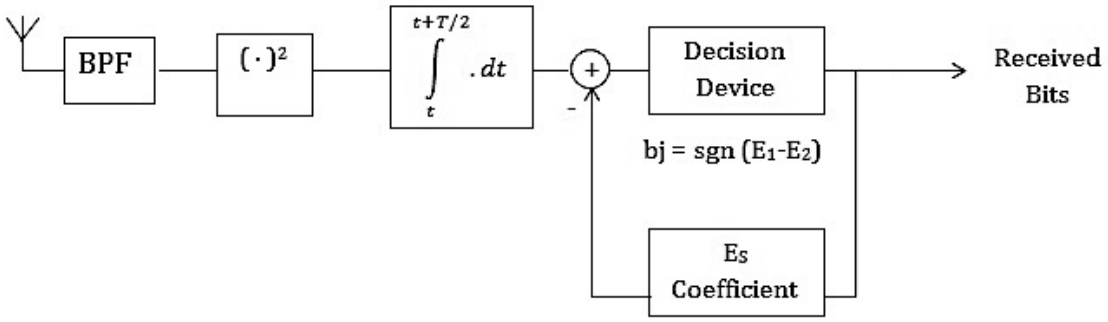

Figure 5-8 : Proposed ED-PPM Receiver with ES based on Iterative Process

In straight comparisons with the structure shown in Figure 5-6, the new iterative structure has no threshold detector block in it and therefore the receiver structure becomes simpler. Initially, three key parameters were needed for the threshold-based pulse subtraction receiver, and here we still follow the same training sequence but measure only 'E_s' to serve the purpose of energy subtraction to cancel out the effects of ISI. The flow of operations for this method is described below.

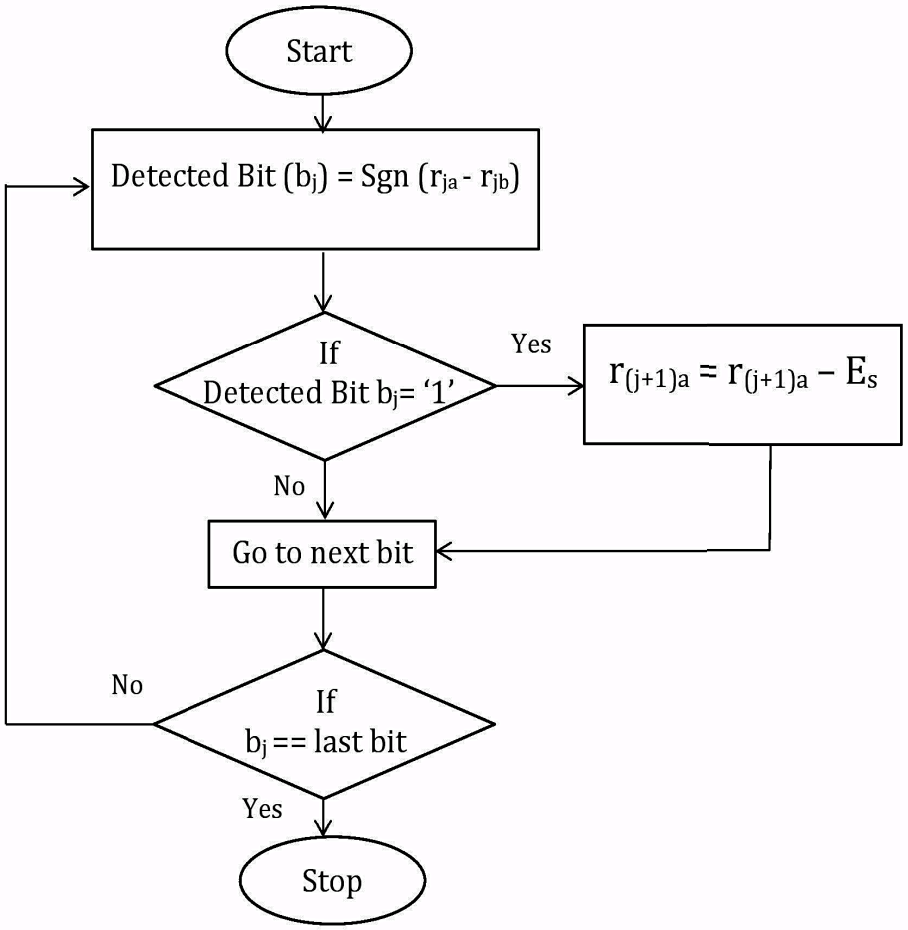

Figure 5-9 : Proposed ED-PPM with ES Iterative Process Flowchart

By rewriting equations from section 5.2.2.3, the received signal is integrated over the limits $[jT_f, jT_f+T_m]$ for first slot of each bit and then from $[jT_f+\delta, jT_f+\delta+T_m]$ for the energy present in the second slot.

$$r_{ja} = \int_{jT_f}^{jT_f+T_m} r^2(t).dt$$

$$r_{jb} = \int_{jT_f+\delta}^{jT_f+\delta+T_m} r^2(t).dt$$

As explained before, the bit decision is purely based on the energies present in both the slots, and the energy subtraction is carried out on the basis of previous decisions and not based on any threshold values.

$$\hat{b}_j = \text{sgn}(r_{ja} - r_{jb})$$

Referring to the flowchart in Figure 5-9, the energy subtraction procedure is carried out in the first slot of the next incoming frame whenever a bit '1' is detected.

$$r_{(j+1)a} = \begin{cases} r_{(j+1)a}, & if\ previous\ bit\ (r_j) = '0' \\ r_{(j+1)a} - E_s, & if\ previous\ bit\ (r_j) = '1' \end{cases} \quad (5.12)$$

From all the above equations, it is clearly evident that the energy subtraction occurs always and only in the first slot of a frame, depending on the value of the previous bit. As a result of this, the new system has shown important gain improvements over the regular energy detector, and also a significant performance increase over the energy detector employing the energy subtraction algorithm with threshold-based pulse detection. The BER Characteristics of this proposed model are explained in the following sections, and also the same will be compared with the other models to show their significance in performance improvements.

5.3 Alternative Method

In this section we propose an alternative model, and investigate this new approach to take advantage of the peak positions of the pulses present in time slots of a PPM-based transceiver without any energy detection, thereby still reducing the complexity of the receiver design and achieving significant results in comparison with the equalization scheme discussed in the above sections. One such method that accomplishes the task is our newly proposed model, the peak detection model, for systems employing the PPM technique.

Numerous trials were performed via computer simulations to check the maximum peak for data pulses and also to check its post-cursor elements leaking in the subsequent slots. It was found that the maximum peaks for the data pulses were mostly greater than the leaking post-cursor elements even with the presence of additive white Gaussian noise (AWGN). Hence, exploiting this condition, it was found that the above conditions were true and the design also produced satisfactory results as discussed in the following sections.

5.3.1 Peak Detection: Block Diagram

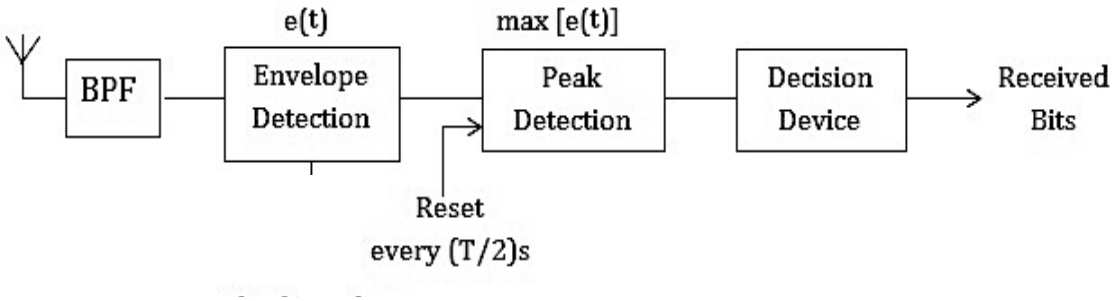

Figure 5-10 : Peak Detection Transceiver Block Diagram

In terms of circuitry, this peak detection transceiver design is less complex than the energy detector, since it does not require any squaring or integrating devices. The low duty cycle is a significant characteristic of IR-UWB, and hence in certain intervals of pulse duration, there is always a peak power associated with the pulse.

The structure of the receiver consists of a BPF and an amplifier at the first stage, and then the process of envelope detection is carried out in the second phase before it is passed to the peak detection circuitry where pulse peak decision occurs. Finally, comparing the peak of the two slots in a PPM frame, the bit decision is made. Hence, the performance of this non-coherent receiver based on peak detection purely relates to the instantaneous peak power amplitude of the pulse, or the pulse peak amplitude. The peak detector is operated at (T_f/2) seconds, which means that it has to be reset for every (T_f/2) seconds. For every reset there would be a peak power detected and this is stored in a buffer. Hence the two peaks recorded in bit duration of T_f second will be compared, and based on the position of the maximum peak, the bit decision is made. This is explained in the following steps:

1. Band pass filtering of the received signal:

$$\hat{y}(t) = BPF\left\{\hat{r}(t)\right\} \tag{5.13}$$

2. Determine the envelope for the signal $\hat{y}(t)$ via modulus operation and then with low-pass filtering

$$\hat{e}(t) = \left|\hat{y}(t)\right|_{LOWPASS} \tag{5.14}$$

3. Determine the instantaneous peak power of the pulse and store it in a buffer at every T_m=T_f/2 seconds

$$P_1 = \max\left[\hat{e}(t)\right]_{jT_f}^{jT_f+Tm} \tag{5.15}$$

$$P_2 = \max\left[\hat{e}(t)\right]_{jT_f+\delta}^{jT_f+\delta+Tm} \tag{5.16}$$

4. Information Bit Detection:

$$\hat{y}_j = \text{sgn}(P_1 - P_2) \tag{5.17}$$

Simulation results for this peak detection, have given satisfactory gain for both weak ISI and strong ISI conditions when compared to that of a basic energy detector. The BER characteristic of this detector is discussed in the next section.

5.4 Implementation Results and BER Characteristics

In order to mitigate ISI with low system complexity as an alternative to the Energy Detector, the peak amplitudes of data and multipath pulses were investigated. Considerable results were achieved using a maximum peak detector, but with a simple energy subtraction algorithm inbuilt in an Energy Detector, we obtained better results to mitigate ISI as shown in the paragraphs below.

BER Characteristics:

1. BER Performance of ED-PPM, ED-PPM with ES and Peak Detection under NO ISI conditions:

Under no ISI conditions, that is, when $\delta=80ns$, the BER characteristics will be the same for ED-PPM, ED-PPM with ES, and it will be exactly similar to the one shown in Figure 5-1. The peak detector on the other hand, performs better than energy detector at low SNR levels and the energy detector performs better at high SNR levels. Since the peak detector works only on amplitude peaks, the receiver operates in linear region whereas the energy detector operates in a square region. Since orthogonality is unimportant between the pulses, and also the absence of square device makes the receiver to operate in linear region, the BER of peak detector should be optimal under no ISI conditions.

2. BER Performance of ED-PPM, ED-PPM with ES and Peak Detection under weak ISI conditions:

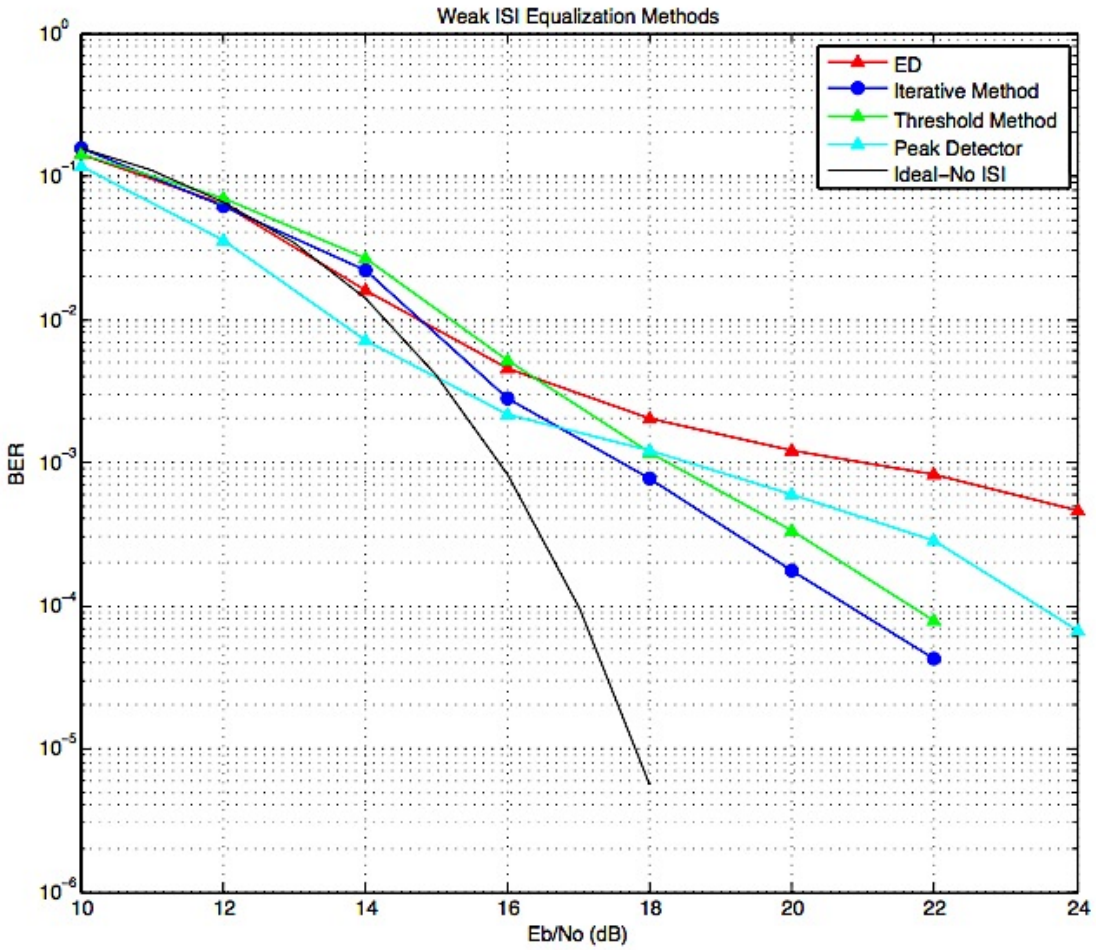

Figure 5-11 : Performance of all receiver designs under weak ISI

For the weak case of ISI, where some of the multipath components overlap onto the next slot, the BER characteristics are shown in Figure 5-10. It is observed that the ED undergoes severe performance degradation. The performance of ED-PPM with ES using threshold or the iterative method are almost similar, the latter being the best out of the two. The peak detector on the other hand achieves significant gain for lower SNR values, but still all the new proposed methods fare relatively better than the basic energy detector.

3. BER Performance of ED-PPM, ED-PPM with ES and Peak Detection under strong ISI conditions:

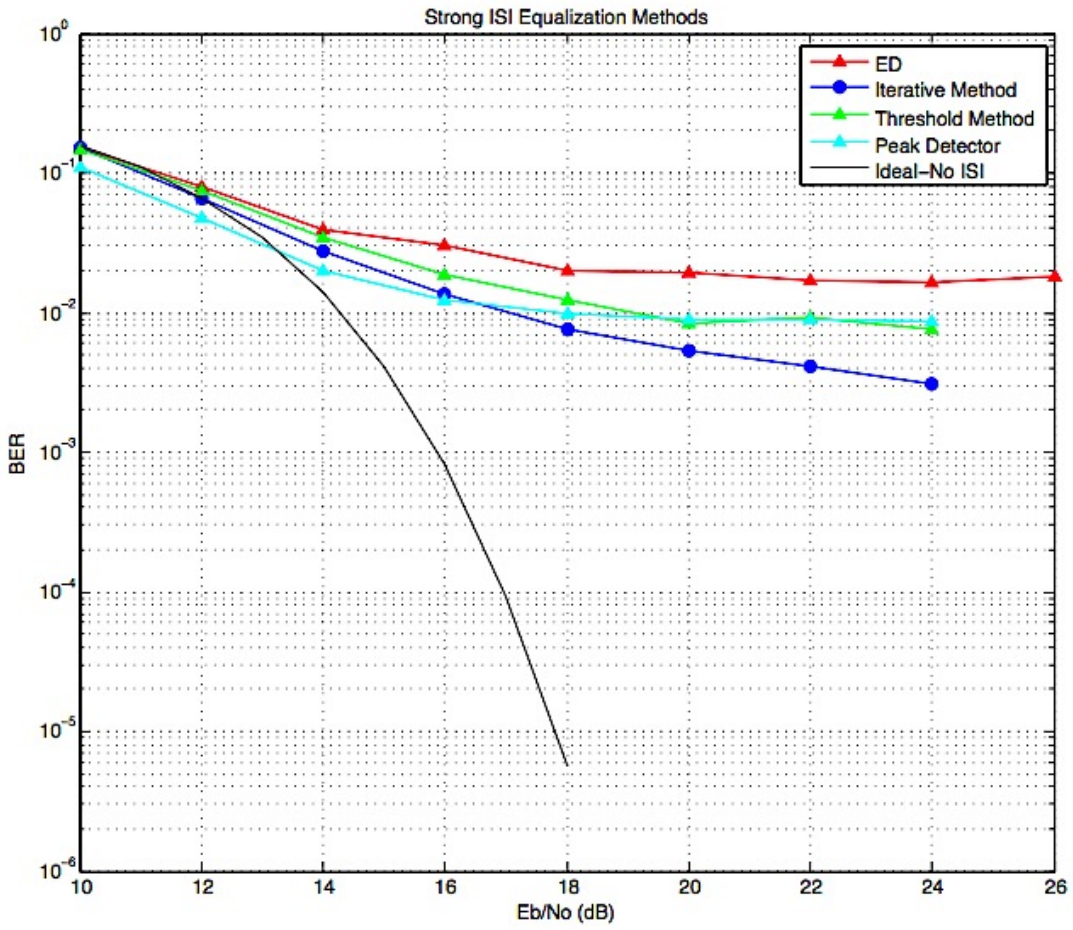

Figure 5-12 : Performance of all receiver designs under strong ISI

The BER characteristics for strong ISI are plotted in Figure 5-11. It is clearly evident that the performance of ED further decreases. All the three proposed receivers perform relatively the same, for lower SNR values, but when the SNR is more than 20db, the ED-PPM using ES with the iterative procedure has achieved significant gain, over all the other methods.

5.5 Comparisons between all three Receiver Designs

Table 5-1 : Performance Comparisons

Performance Analysis	Energy Detection	Max. Peak Detection	E.D. with Energy Subtraction (Threshold Method)	E.D. with Energy Subtraction (Iterative Method)
Multipath Errors	High	Medium	Low	Low
Training Pulses	Not Required	Not Required	Required For E_s and E_{TH}	Required Only for E_s
Modulation	PPM	PPM	PPM	PPM
Performance Weak ISI	Good	Better	Best	Best
Performance Strong ISI	Bad	Good	Better	Best
Performance @ Low SNR	Bad	Very Good	Bad	Good
Complexity	Low	Very Low	Intermediate	Low

A brief comparison on all the receiver designs is summarized in Table 5-1. The ED-PPM with energy subtraction has proved to be effective in operating under both weak and strong ISI conditions. Due to the fact that only E_s is required for the functionality of our new algorithm, the complexity of the receiver is still low. It can also be concluded from the BER results that, the peak detector is well suitable for applications that operate at low SNR levels. This peak detector is only an alternative method, and it demonstrates its superiority over energy detector at low SNR values irrespective of ISI conditions.

CHAPTER 6: CONCLUSIONS

This thesis has presented a novel energy subtraction algorithm for ED-PPM detectors. Two approaches were realized based on this algorithm, where one method was operating at half symbol level and the other operating at full symbol level. The primary focus of this thesis was on receiver structures in order to overcome the effects of ISI due to channel maximum excess delay in IR-UWB receiver structures employing energy detection. An alternative method was also discussed in this thesis to compare the performance of ED-PPM in the presence of ISI. The main objective of this thesis was to design a simple receiver structure that can mitigate ISI at receiver level and to avoid complex signal processing methods.

The design and results of the proposed energy subtraction algorithm have been developed and examined. Inspired from the principles of decision feedback equalization, energy subtraction algorithm was proposed to mitigate ISI at both half symbol and full symbol level for ED-PPM detectors. Instead of employing complex signal processing algorithms to measure the filter coefficients, this thesis proposed training sequences to measure the filter coefficient for the varying channel conditions. This coefficient was then used as the energy subtraction coefficient to mitigate ISI. Since the CM1 model has only post-cursor elements causing ISI, only a feedback filter is used. The decision device makes comparison between the energy levels from two slots present in the bit period and hence a model to cancel the effects of ISI from the previous time slot was designed considering the impact of leaking energy from the pulse present in the previous time slot. The overall structure was then slightly modified and proposed as the second method in order to overcome the limitations of unnecessary subtraction of slot energies.

The proposed methods were implemented using MATLAB programming tool and extensive simulations were performed using the same tool. Significant results were achieved and BER comparisons were made for each receiver design. Thus, a simple ED-PPM detector employing energy subtraction algorithm was designed and the effects of ISI was mitigated effectively.

6.1 Future Work

Prospective research work can be carried out in the future and it is outlined in the following aspects:

- The ED-PPM with energy subtraction should be tested in various channel environments including CM2, CM3 and CM4.
- The channel model used in this thesis has static conditions and hence channel parameters do not change during simulations. Adding a more realistic indoor channel by including some time varying properties could be considered.
- Further investigation can be carried out to avoid unnecessary energy subtraction in the first proposed model operating at half frame level.
- A hardware test bed could be set up to verify simulation results and can be useful for hardware implementations.
- Recently our research group proposed Differential Code Shifted Reference (DCSR) receiver structure that has very good BER characteristics compared to all other available schemes including ED-PPM. Implementation of energy subtraction in DCSR could be investigated and verified.

References

[1] H. Nikookar and R. Prasad, Introduction to Ultra Wideband for Wireless Communications, Springer 2009.

[2] L. Reggiani and G. M. Maggio, "Coherent vs. Non-Coherent Detection for Orthogonal Convolutional Modulation: A Trade-Off Analysis", *in Proc. Of IEEE International Conference on Ultra-Wideband*, pp. 43-48, September 2006.

[3] D. Chunjie, P. Orlik, Z. Sahinoglu, and A. F. Molisch, "A Non-Coherent 802.15.4a UWB Impulse Radio", *in Proc. of IEEE International Conference on Ultra-Wideband*, pp. 146-151, September 2007.

[4] F. Troesch, C. Steiner, T. Zasowski, T. Burger, and A. Wittneben, "Hardware Aware Optimization of an Ultra Low Power UWB Communication System", *in Proc. of IEEE International Conference on Ultra-Wideband*, pp 174-179, September 2007.

[5] A. Rabbachin, L. Stoica, S. Tiuraniemi, and I. Oppermann, "A Low Cost, Low Power UWB Based Sensor Network", International Workshop on Wireless Ad-Hoc Networks, pp 84-88, May 2004.

[6] A. Gerosa, M. Costa, A. Bevilacqua, D. Vogrig, and A. Neviani, "An Energy-Detector for Non-Coherent Impulse-Radio UWB Receivers", *in Proc. of IEEE International Symposium on Circuits and Systems*, pp 2705-2708, May 2008.

[7] F. Troesch and A. Wittneben, "MLSE post detection for ISI Mitigation and Synchronization in UWB Low Complexity Receivers", *in Proc. of IEEE Vehicular Technology Conference*, pp. 2915-2919, April 2007.

[8] R. Prasad, "Candidate Air Interfaces and Enhancements", IST-507102, My Personal Adaptive Global NET (MAGNET), deliverable D3.2.2a, October 2004.

[9] F. Nekoogar, Ultra-wideband Communications: Fundamentals and Applications, Upper Saddle River: NJ: Prentice Hall Professional Technical Reference, 2005.

[10] A. Batra et al., ‘‘Multi-Band OFDM Physical Layer Proposal for IEEE 802.15 TaskGroup 3a,’’ Doc. IEEE P802.15-03/268r3, Mar. 2004; Online resource: http://www.ieee802.org/15/ pub/2003/Jul03/03268r3P802-15_TG3a-Multi-band-CFP-Document.doc

[11] A. Batra et al., “Multi-band OFDM Physical Layer Proposal,” Doc. IEEE802.15-03/267r5, July 2003.

[12] A. Batra et al., ‘‘Design of a Multiband OFDM system for realistic UWB channel environments,’’ *IEEE Transactions on Microwave Theory and Techniques*, vol. 52, no. 9, Part 1, September 2004, pp. 2123–2138.

[13] J. Foerster et al., “Channel modeling sub-committee report final,” IEEE P802.15 Wireless Personal Area Networks, P802.15-02/490r1-SG3a, Feb. 2003.

[14] A Saleh and R. V alenzuela, “A statistical model for indoor multi-path propagation,” *IEEE Journal on Selected Areas in Communications*, vol. 5, pp. 128- 137, Feb. 1987.

[15] I. Opperman, M. Hamalainen and J. Iiatti, UWB Theory and Applications, John Wiley & Sons Ltd., 2004.

[16] H. Reed, An Introduction to Ultra Wideband Communication Systems, Prentice Hall, NJ., 2006.

[17] F. Nekoogar, Ultra-Wideband Communications, Prentice-Hall, NJ. 2006.

[18] R. Hoctor and H. Tomlinson, "Delay-Hopped Transmitted-Reference RF Communications," *in Proc. of 2002 IEEE Conference on Ultra Wideband Systems and Technologies*, pp. 265-269, 2002.

[19] J. Romme and G. Durisi, "Transmit reference impulse radio systems using weighted correlation," *in Proc. International Workshop on Ultra Wideband Systems, Joint with Conf. Ultra wideband Systems and Technologies*, pp. 141-145, May 2004.

[20] D. Goeckel and Q. Zhang, “Slightly frequency-shifted reference ultra-wideband (UWB) radio: TR-UWB without the delay element,” *in Proc. IEEE Military Communications Conf.*, Vol. 5, pp.3029-3035, October 2005.

[21] F. Dowla, F. Nekoogar and A. Spiridon,‘‘Interference mitigation in Transmit-Reference Ultra-Wideband receivers,’’ *IEEE International Symposium on Antenna and Propagation*, 2004, pp. 1307–1310.

[22] D. Lowe, "RF Transceiver for Code-Shifted Reference Impulse-Radio Ultra-Wideband (CSR IR-UWB) System," MASc thesis, Dept. Elect. Eng., Dalhousie Univ., Halifax, NS, 2010.

[23] D. Goeckel and Q. Zhang, “Slightly Frequency-Shifted Reference Ultra-Wideband (UWB) Radio”, *IEEE Transactions On Communications,* Vol. 55, No. 3, March 2007.

[24] H. Nie and Z. Chen, "Code-shifted reference ultra-wideband (UWB) radio," *in Proc.6th Annual Conf. Communication Networks and Services Research*, pp. 385-389, May 2008.

[25] V. Lottici, A. N. D’Andrea, and U. Mengali, “Channel estimation for ultra-wideband communications,” *IEEE Journal on Selected Areas in Communications*, vol. 20, no. 9, pp. 1638–1645, December 2002.

[26] C. Carbonelli, U. Mengali, and U. Mitra, “Synchronization and channel estimation for UWB signals,” *in Proc. IEEE Globecom*, San Francisco, US, December 2003.

[27] J. Romme and K. Witrisal, “Oversampled weighted autocorrelation receivers for transmitted-reference UWB systems,” *in Proc. IEEE Vehicular Technology Conference*, VTC Spring, Stockholm, Sweden, May 30, June 1 2005.

[28] M. Weisenhorn and W. Hirt, “Robust non-coherent receiver exploiting UWB channel properties,” *in Proc. IEEE UWBST*, Kyoto, Japan, May 2004.

[29] E. Arias-de-Reyna, A. D'Amico, and U. Mengali, “UWB Energy Detection Receivers with Partial Channel Knowledge,” *in Proc. of IEEE ICC 2006*, vol. 10, pp. 4688-4693, June 2006.

[30] H. Nie, W. Xiang, Z. Chen, “Performance evaluations of Impulse Radio UWB transceivers requiring no channel estimation under Intra-Vehicle environments,” 2012.

[31] P. A. Bello and B.D. Nelin, “The effects of frequency selective fading on the binary error probabilities of incoherent and differentially coherent matched filter receivers,” *IEEE Trans. Commun. Syst.*, Vol 11, pp. 170–186, June 1963.

[32] S. Gurunathan and K. Feher, “Multipath simulation models for mobile radio channels,” *in Proc. of IEEE Vehic. Technol. Conf.,* pp. 131–134, May 1992.

[33] Q. Wan, "Adaptive RAKE Receiver Structures for Ultra Wide-Band Systems," MSc thesis, Dept. Elect. Eng., Univ. of Saskatchewan, Saskatoon, SK, 2005.

[34] R. Hoctor and H. Tomlinson, “Delay-Hopped Transmitted-Reference RF Communications,” *in Proc. of IEEE Ultra-Wideband Syst. Technol.Conf.*, pp. 265–270, May 2002.

APPENDIX

MATLAB CODE:

Simulator:

```
clear all; close all; clc;

%-------------------------------------------------------------
fileName='mainshiftstrong_EDPPM.txt';
%-------------------------------------------------------------
EbNo=10:2:24;
maxErrs=100;maxBits=1E6;
for i=1:length(EbNo)
    TotalErrs=0; TotalBits=0;
    while((TotalErrs<maxErrs)&&(TotalBits<maxBits))
        [NumErr,NumData]=ED_PPMshift_ES(EbNo(i));
        TotalErrs=TotalErrs+NumErr;
        TotalBits=TotalBits+NumData;
        SavingProcess(EbNo(i),max(EbNo),TotalErrs,maxErrs,fileName);
    end
    BER(i)=TotalErrs/TotalBits;

%-------------------------------------------------------------
save EDPPMshiftstongISI_EQ BER EbNo %% save EDPPMshiftweakISI_EQ for
weak ISI
%-------------------------------------------------------------

end

%-------------------------------------------------------------
delete main_EDPPMshiftstrong.txt
%-------------------------------------------------------------



%-------------------------------------------------------------
delete main_EDPPMshiftstrong.txt
%-------------------------------------------------------------
```

Main Program: (DFE based Iterative Method)

```
function [NumErr_ED,NumData]=ED_PPMshift_ES(EbNo)
%% Initialization
load pulses.mat;
load BPF500.mat;

NumBits=100;
Fs=32e9;
Tb=120e-9;  %Value set for weak ISI; Tb should be set to 80e-9 for
strong ISI
```

```
Tm=Tb/2;
Tf=Tb/2;
Tr=Tb/2;
tr=floor(Fs*Tr);%Pulse repitition Period

L_BPF=length(Bpf500M);
SamNum_Tf=floor(Tf*Fs)+1;

shift=SamNum_Tf-tr;
NumData=0;
NumErr_ED=0;
Thresh=1.0;
[ES_Coeff,~]=Coeff(Fs,Tb,Tm,Tf,pulse); %% Estimation of Subtraction
Coefficient


for ch=1:num_h


%% Generation Of Bits

Bits=randi([0,1],1,NumBits);
for i=1:length(Bits)% Bit-to-Data Mapping
    if Bits(i)==1
        TransData(2*i-1:2*i)=[0 1];
    else
        TransData(2*i-1:2*i)=[1 0];
    end
end
ppmdata=TransData;


%% Modulation Process

channel=pulse_cm1(ch,:);
channel=channel(1:1920);
L=length(channel);

m=length(ppmdata);
n=m*SamNum_Tf;
ModSignal=zeros(m,n);

for i=1:m
    StartIndex=(i-1)*SamNum_Tf+1;
    EndIndex=i*SamNum_Tf;
    ModSignal(i,StartIndex:EndIndex)=channel*ppmdata(i);
end

for j=2:m
    ModSignal(j,:)=circshift(ModSignal(j,:), [1 -((j-1)*shift)]);
end

TransSignal=sum(ModSignal);
TransSignal=TransSignal(1:(m*tr));
TransSignal=[zeros(1,L_BPF) TransSignal];% add zeros of length of BPF
due to noise introduced by it
```

```
%% AWGN Channel

EbNo_Linear=10^(EbNo/10);
A_noise=sqrt(1/(2*EbNo_Linear));
Noise=A_noise*randn(1,length(TransSignal));
ReceivedSignal=TransSignal+Noise;



%% Receiver BPF

FilteredSignal=fftfilt(Bpf500M,ReceivedSignal);
FilteredSignal=FilteredSignal(L_BPF+1:end);



%% Energy Detection with Energy Subtraction

SquareSignal=FilteredSignal.^2;
for i=1:length(ppmdata)
    StartIndex=(i-1)*tr+1;
    EndIndex=i*tr; %Set intergrate time as Tm=Tr
    ReceivedData(i)=sum(SquareSignal(StartIndex:EndIndex));%To obtain
the data energy
    TestData(i)=sum(SquareSignal(StartIndex:EndIndex));
end


for i=1:NumBits
    if TestData(2*i-1)>TestData(2*i)
        ReceivedBits(i)=0;
    else
        ReceivedBits(i)=1;
    end
end

for i=1:NumBits
    if ReceivedBits(i)==1
        TestData(2*i+1)=TestData(2*i+1)-ES_Coeff;
    end
end


%% Demodulation

for i=1:NumBits
    if TestData(2*i-1)>TestData(2*i)
        ReceivedBits(i)=0;
    else
        ReceivedBits(i)=1;
    end
end
```

```
%% Bit Error Rate Calculation
[nerr,~]=biterr(Bits,ReceivedBits);
NumErr_ED=NumErr_ED+nerr;
NumData=NumData+NumBits;
end
end
```

Main Program: (ED-PPM Threshold Method)

```
function [NumErr_ED,NumData]=ED_PPM_Thresh(EbNo)
%% Initialization
load pulses.mat;
load BPF500.mat;

NumBits=100;
Fs=32e9;
Tb=120e-9;  %Value set for weak ISI; Tb should be set to 80e-9 for
strong ISI
Tm=Tb/2;
Tf=Tb/2;
Tr=Tb/2;
tr=floor(Fs*Tr);%Pulse repitition Period

L_BPF=length(Bpf500M);
SamNum_Tf=floor(Tf*Fs)+1;

shift=SamNum_Tf-tr;
NumData=0;
NumErr_ED=0;
Thresh=1.0;
[Thresh_Coeff,~]=Coeff(Fs,Tb,Tm,Tf,pulse); %% Estimation of Subtraction
Coefficient


for ch=1:num_h  % For all 100 possible channels


%% Generation Of Bits

Bits=randi([0,1],1,NumBits);
for i=1:length(Bits)% Bit-to-Data Mapping
    if Bits(i)==1
        TransData(2*i-1:2*i)=[0 1];
    else
        TransData(2*i-1:2*i)=[1 0];
    end
end
ppmdata=TransData;


%% Modulation Process
```

```
channel=pulse_cm1(ch,:);
channel=channel(1:1920);
L=length(channel);

m=length(ppmdata);
n=m*SamNum_Tf;
ModSignal=zeros(m,n);

for i=1:m
    StartIndex=(i-1)*SamNum_Tf+1;
    EndIndex=i*SamNum_Tf;
    ModSignal(i,StartIndex:EndIndex)=channel*ppmdata(i);
end

for j=2:m
    ModSignal(j,:)=circshift(ModSignal(j,:), [1 -((j-1)*shift)]);
end

TransSignal=sum(ModSignal);
TransSignal=TransSignal(1:(m*tr));
TransSignal=[zeros(1,L_BPF) TransSignal];% add zeros of length of BPF
due to noise introduced by it



%% AWGN Channel

EbNo_Linear=10^(EbNo/10);
A_noise=sqrt(1/(2*EbNo_Linear));
Noise=A_noise*randn(1,length(TransSignal));
ReceivedSignal=TransSignal+Noise;



%% Receiver BPF

FilteredSignal=fftfilt(Bpf500M,ReceivedSignal);
FilteredSignal=FilteredSignal(L_BPF+1:end);



%% Energy Detection with Energy Subtraction

SquareSignal=FilteredSignal.^2;
for i=1:length(ppmdata)
    StartIndex=(i-1)*tr+1;
    EndIndex=i*tr; %Set intergrate time as Tm=Tr
    ReceivedData(i)=sum(SquareSignal(StartIndex:EndIndex));%To obtain
the data energy
    TestData(i)=sum(SquareSignal(StartIndex:EndIndex));
end


%% ED-PPM with ES Operation
```

```
for i=1:(m-1)
    if TestData(i)>EnergyThresh
        TestData(i+1)=TestData(i+1)-Thresh_Coeff;
    end
end


%% Demodulation

for i=1:NumBits
    if TestData(2*i-1)>TestData(2*i)
        ReceivedBits(i)=0;
    else
        ReceivedBits(i)=1;
    end
end


%% Bit Error Rate Calculation

[nerr,~]=biterr(Bits,ReceivedBits);
NumErr_ED=NumErr_ED+nerr;
NumData=NumData+NumBits;
end
end
```

Main Program : (Peak Detection)

```
function [NumErr_ED,NumData]=Max_Peak_Detector(EbNo)

%% Initialization
load pulses.mat;
load BPF500.mat;

NumBits=100;
Fs=32e9;
Tb=160e-9;
Tm=Tb/2;
Tf=Tb/2;
Tr=Tb/2;

tr=floor(Fs*Tr);%Pulse repitition Period

L_BPF=length(Bpf500M);
SamNum_Tf=floor(Tf*Fs);

shift=SamNum_Tf-tr;
NumData=0;
NumErr_ED=0;
for ch=1:num_h

%% Generation Of Bits
TransBits=randi([0,1],1,NumBits);
```

```
for i=1:length(TransBits)% Bit-to-Data Mapping
    if TransBits(i)==1
        TransData(2*i-1:2*i)=[0 1];
    else
        TransData(2*i-1:2*i)=[1 0];
    end
end
ppmdata=TransData;

%% Modulation Process
channel=pulse_cm1(ch,:);
channel=channel(1:2560);
L=length(channel);

m=length(ppmdata);
n=m*SamNum_Tf;
ModSignal=zeros(m,n);

for i=1:m
    StartIndex=(i-1)*SamNum_Tf+1;
    EndIndex=i*SamNum_Tf;
    ModSignal(i,StartIndex:EndIndex)=channel*ppmdata(i);
end

for j=2:m
    ModSignal(j,:)=circshift(ModSignal(j,:), [1 -((j-1)*shift)]);
end

TransSignal=sum(ModSignal);
TransSignal=TransSignal(1:(m*tr));
TransSignal=[zeros(1,L_BPF) TransSignal];% add zeros of length of BPF
due to noise introduced by it

%% AWGN Channel
EbNo_Linear=10^(EbNo/10);
A_noise=sqrt(1/(2*EbNo_Linear));
Noise=A_noise*randn(1,length(TransSignal));
ReceivedSignal=TransSignal+Noise;

%% Receiver BPF
FilteredSignal=fftfilt(Bpf500M,ReceivedSignal);
FilteredSignal=FilteredSignal(L_BPF+1:end);
PSignal=abs(FilteredSignal);

%% Peak Detection
for i=1:length(ppmdata)
    StartIndex=(i-1)*tr+1;
    EndIndex=i*tr; %Set intergrate time as Tm=Tf
    ReceivedData(i)=max(PSignal(StartIndex:EndIndex));%To obtain the
data energy
end

%% Bit Detection
for j=1:NumBits
    if ReceivedData(2*j-1)>ReceivedData(2*j)
        ReceivedBits(j)=0;
```

```
    else
        ReceivedBits(j)=1;
    end
end

%% Bit Error Rate Calculation
[nerr,~]=biterr(TransBits,ReceivedBits);
NumErr_ED=NumErr_ED+nerr;
NumData=NumData+NumBits;
end
end
```

Saving Process : (common for all three designs)

```
function SavingProcess(EbNo,maxEbNo,TotalErrs,maxNumErrs,fileName)
process=TotalErrs/maxNumErrs*100;
if process>100
    process=100;
end
fid=fopen(fileName,'w');
fprintf(fid,'\nProcessed %2.2f%s @ Eb/No=%d /%d.',...
    process,'%',EbNo,maxEbNo);
fclose(fid);
```

Plotting of BER curves:

```
clear all; close all; clc;

h=figure; % plot the needed figure

load EDPPM_ES_weak.mat;
f(1)=semilogy(EbNo(1:length(BER)),BER,'r^-');hold on;
set(f(1),'MarkerFaceColor','R');

load EDPPM_DFE_weak.mat;
f(2)=semilogy(EbNo(1:length(BER)),BER,'bo-');hold on;
set(f(2),'MarkerFaceColor','B');

load EDPPMshift_weak.mat;
f(3)=semilogy(EbNo(1:length(BER)),BER,'g^-');hold on;
set(f(3),'MarkerFaceColor','G');

load Peak_Detector_weak.mat;
f(4)=semilogy(EbNo(1:length(BER)),BER,'w^-');hold on;
set(f(4),'MarkerFaceColor','W');



% Theoritical Analysis
EbNo=(10:18);
fig=0;
alpha=1;
fL=3.7e9;
fH=4.2e9;
```

```
TM=80e-9;

Eb=1;
No=10.^(-EbNo/10);
BER_theory=0.5*erfc(alpha*Eb./(2*(sqrt(alpha*Eb*No+No.^2*(fH-
fL)*TM))));
f(5)=semilogy(EbNo,BER_theory,'k-');
set(f(5),'MarkerFaceColor','K');


fl=legend([f(1:end)],'ED','Iterative Method', 'Threshold Method', 'Peak
Detector', 'Ideal-NoISI');


set(fl,'orientation','vertical');hold on;
title('Weak ISI Equalization Methods');
xlabel('Eb/No (dB)');ylabel('BER');grid on;set(gcf,'color','w');hold
on;
```